uOttawa

L'Université canadienne
Canada's university

FACULTÉ DES ÉTUDES SUPÉRIEURES ET POSTOCTORALES

u Ottawa

L'Université canadienne
Canada's university

FACULTY OF GRADUATE AND POSDOCTORAL STUDIES

Daniel Zysman
AUTEUR DE LA THÈSE / AUTHOR OF THESIS

M.Sc. (Biology)
GRADE / DEGREE

Department of Biology
FACULTÉ, ÉCOLE, DÉPARTEMENT / FACULTY, SCHOOL, DEPARTMENT

The Role of Neuronal Feedback in the Detection of Transient Signals : A Computational Approach

TITRE DE LA THÈSE / TITLE OF THESIS

J. Lewis
DIRECTEUR (DIRECTRICE) DE LA THÈSE / THESIS SUPERVISOR

CO-DIRECTEUR (CO-DIRECTRICE) DE LA THÈSE / THESIS CO-SUPERVISOR

S. Aris-Brosou

A. Longtin

J. Dawson

Gary W. Slater
Le Doyen de la Faculté des études supérieures et postdoctorales / Dean of the Faculty of Graduate and Postdoctoral Studies

The role of neuronal feedback in the detection of transient signals: a computational approach

Daniel Zysman

Thesis submitted to the
Faculty of Graduate and Postdoctoral Studies
University of Ottawa

In partial fulfilment of the requirements for the degree of
Masters of Science in Biology

Ottawa-Carleton Institute of Biology

Thèse soumise à
la Faculté des Etudes Supériures et Postdoctorales
Université d'Ottawa

En vue de l'obtention de la
Maitrîse en Sciences Biologiques

L'Institut de Biologie d'Ottawa-Carleton

Your file Votre référence
ISBN: 978-0-494-74165-8
Our file Notre référence
ISBN: 978-0-494-74165-8

Table of contents

List of figures

List of tables

List of abbreviations

AM	Amplitude modulation
AUC	Area under the curve
CLS	Centrolateral segment
CMS	Centromedial segment
DP	Deep pyramidal cell
EER	Equal error rate
EGp	Eminentia granularis posterior
ELL	Electrosensory lateral line lobe
EOD	Electric organ discharge
LIF	Leaky integrate and fire neuron
LS	Lateral segment
nP	Nucleus praeminentialis
ROC	Receiver operating characteristic
SD	Standard deviation
S.E.	Standard error
SP	Superficial pyramidal cell

Abstract

This study investigates the role of neuronal feedback in the detection of small amplitude transient signals. We focus specifically on how the weakly electric fish *Apteronotus leptorhynchus* capture prey such as *Daphnia* in a noisy environment, by means of its electric sense. Using the electrosensory network as a template, we build a computational model that allows us to evaluate detection performance in two different scenarios: without neuronal feedback (open-loop) and with neuronal feedback (closed-loop). For each network scenario, spike count distributions across realizations are computed in the absence and presence of the prey-related signal, and compared using ROC (Receiver Operating Characteristic) curves analyses. The area under the ROC curve (AUC) and the equal error rate (EER) are used to quantify the performance of the different network configurations.

For body-object distances < 20 mm, the closed loop model results in a more robust and reliable signal detection than the open loop configuration. For larger distances, there are no differences between open and closed loop. These results depend on the exact choice of parameters for the model, in particular those controlling feedback inhibitory input strength; increasing inhibition, to a certain extent, further improves the closed-loop model. This study shows, in a simplified model framework that can be applied to a variety of sensory systems, how feedback can enhance the detection of weak transient signals.

Résumé

Cette étude vise à déterminer le rôle de la rétroaction neuronale lors de la détection des petits signaux transitoires. Nous nous concentrons spécifiquement sur la façon dont les poissons faiblement électriques, *Apteronotus leptorhynchus*, capturent des proies tel que les daphnés dans un environnement bruyant à l'aide de leur sens électrique. En utilisant un réseau électrosensoriel comme une matrice, nous avons construit un modèle computationnel qui nous permet d'évaluer la performance de détection lors de deux scénarios : avec la rétroaction neuronale (boucle fermée) et sans celle-ci (boucle ouverte). Pour chaque scénario du réseau, les distributions des comptes des pics durant les réalisations ont été calculées en présence et en absence des signaux liées au proies, puis comparées selon les analyses des courbes ROC (Caractéristique de Fonctionnement du Récepteur). L'aire sous la courbe ROC et le taux d'erreur égalisé ont servi à quantifier la performance des différentes configurations du réseau.

Pour des distances entre le corps du poisson et l'objet de moins de 20mm, le modèle de la boucle fermée permet de détecter les signaux de façon plus exacte et plus précise que la configuration en boucle ouverte. Ces résultats dépendent du choix exacte des paramètres du modèle, en particulier ceux contrôlant la force des rétroactions inhibitrices; augmenter l'inhibition améliore jusqu'à un certain point le modèle de la boucle fermée. Cette étude montre, dans le cadre d'un modèle simplifié ce qui peut être appliqué à une variété de systèmes sensoriels et comment la rétroaction peut améliorer la détection de faibles signaux transitoires.

Acknowledgments

In the first place, a big thanks to John Lewis, my thesis supervisor, for his generosity both intellectual and financial, for his support, guidance and patience through the long and winding road of this adventurous thesis. Also, for always being optimistic, kind and helpful; particularly in the moments when one seems to don't find the path. For these reasons a debt of gratitude will remain forever.

Thanks to the memebers of my advisory committee, for refreshing ideas and guidance: Andre Longtin, Michael Jonz and Jeff Dawson.

To the members of the Lewis lab, both past and present: Ginette, Colleen, Isabelle, Pascale, Katie, Agnes, Mayron, Nick, Jad, Alan, Julie, Gerri, Sally, Zhaohong, Emilie, Phil, Pierce and Mike. A special note to those who made a remark on my own personality and help me to adapt to a new environment. A distinction should be made for Wudu Lado: a true friend, supportive in the good and the bad moments, a good advisor, and an impeccable source to learn new English vocabulary. I am going to miss our lunches and crosswords as well as all the fun we had outside the lab. Also a big thanks to the members of the efish community in Ottawa, notably, Gary, Will, Jeremie, Ben, and Na; and particularly to Erik Harvey Girard, for very interesting conversations on politics, literature, science and for allow me to practice my poor French always with a smile in his face. Also, thanks for doing a superb translation on the abstract for this thesis.

To my friends in the Biology Department: the invincible D'Iorio gang for awesome lunches and other memorable moments, as well as for let me appreciate human diversity and in that way lead me to forge a better person. To Eric Vaillancourt- for great conversations over wine, beer and cheeses-, Hector Vazquez Rivera- for being a very supportive friend and perhaps one of the most interesting interlocutors I had in Ottawa-, and Houman Ghasriani, a very funny friend, politically inspiring and a brother in spirit.

Also to the friendly and welcoming Scaiano troupe: Lili, Nati, Marta, Paco, Raque, Vero, Emilio and Maria. For keeping the Spanish and Latino essence alive. For good BBQ's, and other enjoyable and pleasant outings. A final note to Mark Baxter, a great roommate and connoisseur on movies, and to Charly Featherston, for his invaluable help during my first months in Ottawa and for always being available in case of need.

To the executive council and stewards body of CUPE 2626 for showing in various occasions that change in this world is not utopian.

To Mike Murphy and Ian Myers at the electronics shop, for saving my laptop in a crucial moment.

To Tammy Rodela, Andrey Massarsky, Yves Genest, John Lewis, Katie Gilmour, Steve Perry, Collin Montpetit and John Basso; for wonderful and enjoyable teaching experiences.

A special remark to those who host me during my last months in Ottawa. Dimitri and Paula, thanks for your generosity. Lisa and Taleen, thanks for your hospitality and fun moments together.

To my friends abroad, for keeping the ties and memories of good times in university and life: Tami, Diegui, Lu, Nouki, Mayra, Juan y Ramiro.

Last but not least, to my family spread over Argentina, Colombia, USA, Israel, Germany and Angola. Thanks for your unconditional support and encouragement. Thanks to my mother, for her love and passion. And thanks to my father, for being an infinite source of inspiration and ideas. Thanks for your support, patience and understanding.

Al mar eché un poema

Que llevó con el mis preguntas y mi voz

Como un lento barco, se perdió en la espuma.

Le pedí que no diera la vuelta

Sin haber visto el altamar

Y en sueños hablar conmigo de lo que vio

Aún si no volviera, yo sabría si llegó

Viajar la vida entera

Por la calma azul, o en tormentas zozobrar

Poco importa el modo si algún puerto espera

Aguardé tanto tiempo el mensaje

Que olvidé volver al mar

Y así yo perdí aquel poema

Grité a los cielos todo mi rencor

Lo hallé por fin, escrito en la arena

Como una oración

El mar golpeó en mis venas

Y libró mi corazón.

Pedro Aznar
Dream of the return

Chapter I

Introduction

Feedback pathways are ubiquitous, and thus a central and important feature of brain organization. The precise and exact roles of feedback pathways are in general very difficult to study due to the inherent complex dynamics of closed-loop systems. These complexities arise from the interplay of three important phenomena:

- delays in the feedback signal.
- the variable degrees of synaptic plasticity expressed both in temporal and spatial scales in feedback circuits.
- and the interaction of feedback loops with different signs: on one hand, positive feedback tends to increase the signal that caused it. Positive feedback loops are also known as self-reinforcing loops. On the other hand, negative feedback tends to reduce the signal that generated it, and are therefore known as self-correcting or balancing loops (Rosenblueth et al., 1943; Wiener, 1961).

To fully understand the role of feedback in neural processing, *in vivo* studies preserving intact feedback networks and connections are required. However, this approach usually leads to results that are not easy to understand and interpret, given the high degrees of freedom and the low level of experimental control. One valid alternative to address this issue is to use *in vitro* slices preserving feedback circuits, but this is difficult to achieve due to topological and anatomical constraints. Nonetheless, in some cases this experimental procedure has provided an interesting complement to more realistic *in vivo* studies (e.g. Agmon and Connors, 1992; Mileva et al., 2008). A second alternative is to study feedback networks using a mathematical modelling and computational neuroscience approach. In this thesis we follow this last path. Our focus of study is to understand the role of feedback in the detection of transient sensory signals. By transient we mean relevant biological signals that are restricted

in the spatial-temporal domain, and may be difficult to detect due to low amplitude. As a very interesting and prototypical phenomenon we pick the electrodetection of prey in weakly electric fish, with particular emphasis on the species *Apteronotus leptorhynchus*, the brown ghost knife fish. In the following sections, we introduce the animal model, the problem of prey detection and the role of electrosensory networks in that particular task. Then, we present an overview of the computational network model considered, and the conceptual framework to analyze the model's performance. We then make the case for how such models can lead to better understanding of more general problems where feedback is involved. Finally, we outline our working hypothesis and objectives for this thesis.

1.1 Prey detection in *Apteronotus leptorhynchus*

Gymnotiform weakly electric fish, such as *Apteronotus leptorhynchus*, have been a widespread animal model used to understand neural computation and adaptive sensory filtering (for reviews see: Bastian, 1994; Heiligenberg, 1991; Rose, 2004). These fish inhabit the freshwater systems of Central and South America, particularly the Amazon and Orinoco basins, and are able to navigate and hunt in dark and murky waters by means of an electric organ discharge (EOD) (Moller, 1995). This discharge for *A. leptorhynchus* is produced at a 600 to 1200 Hz constant rate (depending on the individual fish), in a quasi-sinusoidal fashion. Each cycle of the EOD produces a dipole-like electric field of a few millivolts in amplitude that surrounds the fish (Knudsen, 1975). Nearby objects, such as prey, or the interference of electric fields due to the presence of other electric fish, give rise to amplitude modulations (AM) of the fish's own EOD. Specialized electroreceptors, distributed throughout the fish skin, encode these signal modulations.

Primary afferent neurons receive input from the electroreceptors and encode the changes in transdermal potential into a train of action potentials. In fact, there are two anatomically distinguishable types of electroreceptors doing this work. On one hand, ampullary organs respond to low frequency electric fields of extrinsic origin (direct current (DC)-20 Hz); on the other hand, tuberous receptors are specialized in detecting amplitude modulations of the EOD (Zupanc and Bullock, 2005). Certain types of gymnotiforms, as is the case for *Apteronotus*, have a continuous and quasi sinusoidal EOD. In these species, tuberous electroreceptors can be divided into two categories: time coders (T type) and probability coders (P type), based on the firing characteristics of the afferent fiber that innervates them. Both T- and P-type afferents fire at most one action potential per EOD cycle, with spiking times that are phase locked to the EOD cycle. Notably, the phase locking in T units is much stronger and precise than in P units. Furthermore, P units fire irregularly with a per cycle firing probability that is highly dependant on stimulus intensity, whilst T units fire very regularly on every EOD cycle (Scheich et al., 1973). Also, these units differ in the type of information they encode. T units are tuned to detect phase shifts in the stimulus as changes in spike timing, whereas P units encode stimulus amplitude by means of changes in firing probability (Xu et al., 1996). In *Apteronotus*, the vast majority of tuberous receptors found in the trunk region are of the P type (Hagiwara et al., 1965).

Primary electroreceptor afferents penetrate the medulla only from the anterior lateral line nerve and terminate in the deep layers of the electrosensory lateral line lobe (ELL, Carr et al., 1982), the first nucleus in the electrosensory pathway. The ELL in gymnotiforms is a bilateral structure that protrudes laterally from the dorsal medulla (Bell and Maler, 2005). Like the vast majority of sensory systems, electrosensory systems show extensive feedback. Much of the research has been focused on the early stages of the feedback pathways

involving ELL (Berman and Maler, 1999; Sawtell et al., 2005). The principal cells in ELL are the pyramidal cells; these cells receive afferences from the electroreceptors, and also are the target of two sources of feedback, the so-called *direct* and *indirect* pathways (Figure 1.1): the former arises from stellate (excitatory) and bipolar (inhibitory) neurons of the nucleus praeminentialis (nP), and the latter from cerebellar (eminentia granularis posterior, EGp) granule cells via parallel fibers (Sas and Maler, 1983; Sas and Maler, 1987). Another important feature of ELL pyramidal cells is that they exist in two basic types: basilar and non-basilar cells. Basilar pyramidal cells are characterized by a large and thick basal dendrite ending in a dense arborization, whereas non-basilar cells lack basal dendrites (Maler, 1979). At the physiological level, basilar cells respond to increases in EOD amplitude and are thus called E cells (for excitation), and non-basilar cells react to decreases in EOD amplitude, and are referred to as I cells (for inhibition, Saunders and Bastian, 1984). The ELL is further organized into three topographic maps that are spatially segregated within three segments: the centromedial (CMS), the centrolateral (CLS) and the lateral (LS) (Heiligenberg and Dye, 1982). These topographic maps differ not only in the number of pyramidal cells each contain, but more importantly in the size and shape of pyramidal cell receptive fields (Maler, 2009a). It is important to note that ELL pyramidal neurons are the primary source of electrosensory information for the rest of the brain, and thus any processing occurring at this level will have a major influence on electrosensory-mediated behaviours.

Returning to the description of the two main feedback pathways at the ELL level, it is important to mention that not all pyramidal cells participate equally in these circuits. Bastian and collaborators (2004) have shown that one subclass of pyramidal neurons (deep subclass; Figure 1.1, DP) are the primary source of projections to the nP, whereas another subclass, the superficial pyramidal neurons, forms the main projections to higher areas (torus

semicircularis, Figure 1.1, SP). Further, while both subtypes appear to receive feedback via the indirect pathway, it is the superficial subtype that receives the majority of the plastic feedback (Bastian et al., 2004). By plastic we mean that the strength of the synaptic inputs arising from feedback projections can change with time and synaptic activation history. Differential input from the direct feedback pathway has not yet been studied. Future work in slice preparations will be necessary to fully address this question.

At this point, it is important to mention that the direct feedback pathway has been hypothesized to be involved in a sensory searchlight (Berman and Maler, 1999; Bratton and Bastian, 1990). The original proposition of the sensory searchlight hypothesis is based on the visual system (Crick, 1984). It is well known that different areas of the neocortex in primates are maps specialized to extract certain features of the visual scene, and certainly there is binocular integration (Hubel and Wiesel, 1977). However, as we move to the higher brain centers involved in the visual pathway, this mapping becomes more diffuse and cells in those areas respond to more complex features of the visual stimulus. The paradox is that we perceive the visual world as a unity, not as the interaction of different features. So, the question is how this unification arises. Crick (1984) proposed the idea of the sensory searchlight as a possible explanation for this situation. The argument here is that the sensory searchlight mechanism is not shining light on a dark scenario, but rather making a particular feature more noticeable by causing it to "pop out" of the visual landscape. The parallels with the electric sense are clear: presence of topographic maps, feedback loops, and projections to higher brain centers, as well as the functional requirement for feature extraction (Gabbiani et al., 1996; Metzner et al., 1998; Nelson and Maciver, 1999; Wessel et al., 1996). Therefore, given that the direct feedback pathway in the electrosensory network shares many of the properties proposed by Crick as essential to work in a sensory searchlight fashion, it was

hypothesized that this pathway is important to enhance transient signals such as preys (Berman and Maler, 1999). Again, the rationale here is that feedback is enhancing feature extraction or weak stimulus detection in a noisy electrosensory scene. For this reason, we discuss our analyses in the context of the direct feedback pathway in ELL. The model we present is based on E-type pyramidal cells.

1.2 Simplified neural models

As mentioned in the previous section, the central protagonists of the network we are trying to model are the ELL pyramidal cells. These cells have a complex anatomical geometry, and express a wide variety of ionic currents. Thus, trying to model pyramidal cells at this level of detail is computationally expensive, however some interesting approximations can be made without loosing generality (Dayan and Abbott, 2001; Doiron et al., 2002). We plan to model the ELL pyramidal cells as a single compartment leaky integrate and fire neuron (LIF). Let's dissect this expression carefully. To begin with, there is no geometry, shape or anatomical form assumed; all the dimensions of the cell are reduced to a single point in space. To continue, the leaky integrate and fire model (Lapicque, 1907) captures the basic behaviour of neurons, the principle of excitability. A real neuron is characterized by a threshold voltage that has to be surpassed in order to produce an action potential. Once this happens, the action potential occurs, an all-or-none event, and the cell must return to the resting conditions before another event can occur. Lapicque postulated that a very simple circuit consisting of a capacitor and a resistor in parallel can capture this behaviour (Figure 1.2). In this circuit or model, the capacitor mimics the membrane as a charge segregating device, and hence able to integrate inputs or stimuli. The resistor connected to ground acts as

a leakage current that provides a mechanism to discharge the capacitor and allows the modelled cell to "forget" in a proper time scale of any previous stimulation. A closer and analytical perspective on this circuit will allow us to understand how it works.

In accordance to Kirchoff's circuit law, the sum of currents flowing into any node in an electrical circuit is equal to the sum of currents flowing out of that node. This is due to conservation of charge. Using this law -at node A in Figure 1.2- leads to this expression:

$$I_{ext} = I_R + I_C \tag{1.1}$$

that the sum of the currents through the resistor and capacitor (I_R and I_C respectively) is equal to the external current being applied (I_{ext}). Using Ohm's law we find the expression for the current through the resistor is:

$$I_R = \frac{V}{R} \tag{1.2}$$

where V is the voltage difference across the resistor R (in fact this is the voltage difference across the extracellular and intracellular compartments). As previously stated, the capacitor acts as a charge (q) separating device, and the amount of charge it separates is proportional to the capacitance (C) and the voltage difference across its plates (V):

$$q = C \times V \tag{1.3}$$

If we differentiate equation 1.3 with respect to time we get the expression for the capacitive current:

$$I_C = \frac{dq}{dt} = C\frac{dV}{dt} \tag{1.4}$$

Next, we can use equations 1.2 and 1.4 to re-write equation 1.1 in the following way:

$$I_{ext} = \frac{V}{R} + C\frac{dV}{dt} \tag{1.5}$$

and equation 1.5 can be re-arranged in a way to lead to the standard expression for the LIF dynamics:

$$\tau\frac{dV}{dt} = R\,I_{ext} - V \tag{1.6}$$

where τ is the membrane time constant defined as the product of the resistance R and the capacitance C. If more than one current source is present then the first right hand term in equation 1.6 is the summation across current sources times the resistance. Integration of this equation either analytical or numerically would allow us to find the variations of voltage V in time. The dynamics described by equation 1.6 - an ordinary differential equation - are first order if the external current is independent of the transmembrane voltage. In this case the analytical solution is:

$$V(t) = R\,I_{ext}[1 - e^{(-\frac{t}{\tau})}] \tag{1.7}$$

Using this expression, an action potential (or spike) is said to occur when $V(t)$ reaches a threshold V_{thresh}. Just following the action potential, the voltage is reset to a fixed level (mimicking the recovery process) and the cycle starts again. In this way, the timing of the action potentials can be recorded. Of course this simple model cannot produce action potentials (higher order dynamics are required). Nonetheless, this model has been extensively used and has been proven very successful in spite of its simplicity (Abbott, 1999; Brunel and van Rossum, 2007). More realisic dynamics can be incorporated into the LIF model by using currents that are voltage dependant as we would do in the development of our model (see Materials and methods).

In the context of electrosensory processing, LIF neurons have been successfully used in a wide variety of contexts and scales: from single cell analysis to network simulations. An example of the former is the implementation of an LIF model with dynamic threshold that has been able to reproduce the activity of P electroreceptors afferents (Chacron et al., 2001). At the network level, the LIF has been used to study the role of feedback in producing oscillatory activity under spatial diffuse stimulation, such as the communication signals used by weakly electric fish (Doiron et al., 2003). In addition, a recent theoretical study has aimed to understand the mechanisms of feedback-mediated gain control using LIF networks, drawing parallels with electrosensory systems feedback circuitry (Sutherland et al., 2009).

1.3 The role of feedback in other systems

Feedback in control and electronic systems has been widely used for purposes of adaptive filtering and noise cancellation (for examples and applications see: Horowitz and Hill, 1989). An interesting example of the latter is the active noise cancelling headphones.

This headphone has a microphone that picks up environmental noise; an electronic circuit uses that information to produce a signal that has the same frequency content as the noise but is in antiphase with it. Then, the original noise recorded and the output of the circuit are combined to produce negative interference and hence cancel the noise (i.e. noise is cancelled by destructive interference). Interestingly, in *Apteronotus leptorhynchus*, a very similar mechanism involving the indirect feedback pathway cancels reafference inputs (self-stimulation due to animal's own movement) and other predictable signals (Bastian, 1995; 1996; 1999). Modelling efforts have shown the importance of short-term synaptic plasticity in the generation of the negative image for effective reafference suppression (Lewis et al., 2007). Additionally, adaptive filtering is responsible for the cancellation of self-generated noise due to movement in the scorpion fish, *Scorpoena papillosus* (Montgomery and Bodznick, 1994; 1999).

The roles of neuronal feedback have been also studied in mammalian systems. As an example, recent studies using the feedback loops present in the vibrissae sensorimotor system of the rat have shown that those loops are involved in phase sensitive detection as well as in sensory processing optimization (Ahissar and Kleinfeld, 2003; Kleinfeld et al., 2006). It is important to mention that rats locate objects in space by moving their whiskers back and forth in a repetitive fashion. The feedback circuit mentioned allows them to decode properties of the object such as texture, shape and position (Diamond et al., 2008).

Feedback in the context of neural systems has been the focus of many theoretical studies (e.g.: Ermentrout et al., 2001; Laing and Longtin, 2003; Lindner et al., 2005; Ma and Wu, 2007). Important for the purpose of this thesis is the result reported by Chacron and collaborators (2005). They have shown that delayed excitatory and inhibitory feedback can

alter the firing response in modeled stochastic neurons, by creating resonances that could enhance information transmission in certain frequencies bands.

In this context, it is a valid assumption to make that feedback can help in the detection of small amplitude transient signals. In the following section, we present the analytical framework we use to assess the model performance under the task of detecting stimuli mimicking prey.

1.4 Receiver Operating Characteristic curve, assessing models performance

The receiver operating characteristic (ROC) curve is commonly used to estimate the reliability of signal detection (Green and Swets, 1966). It was developed during the Second World War for the analysis of radar signals. In this original context, an operator (hence the name of the technique) had to perform a binary classification task regarding the presence or absence of an enemy in the field according to how many blinks appeared on the radar screen. The main idea of the ROC was to develop a robust statistical method to quantify the performance of different operators, or classifiers, during a signal detection task.

This problem can be easily translated to the scenario we consider in this thesis: making a decision whether a prey-related signal is present or not, and then comparing the performance of different network configurations based on a statistical criterion. In order to do that, we must compare the spike count distributions (these distributions are based on the number of spikes produced in a particular time window over many trials, see section 2.4 for more details), when the prey is absent and when the prey is present. The ROC curve quantifies the trade off between the probability of making a false alarm, this is saying that the

prey was there when it was not, and the probability of making a correct detection, as the threshold for making a decision is varied (Figure 1.3). These probabilities depend on the amount of overlap of the two distributions (presence and absence of stimulus), and where the decision threshold is placed. The ROC curve summarizes this trade off as the threshold is varied from all possible values. The principal diagonal in this type of plot represents the performance of a chance classifier: this is someone that is guessing all the time, with a 50% chance of saying no and 50% chance of saying yes, for object presence. Points above the principal diagonal represent performances that are better than the chance classifier, and the contrary is the case for points below the principal diagonal. The area under the ROC curve (AUC) is a measurement of a classifier's performance (Fawcett, 2006). The chance classifier will have an AUC of exactly 0.5. AUC's above 0.5 indicate better detection performance than the chance detector. Hence, higher values of AUC indicate better performance, with an ideal observer having an AUC of 1 (never making mistakes). It is important to notice that this technique assumes an omniscient observer; this is someone who knows the distributions involved beforehand and thus can exactly calculate the probabilities of making a correct decision or making a mistake with its inferential rule.

Another usual measurement when performing ROC analyses is the so-called equal error rate (EER, Figure 1.4); here it is assumed that the observer has an equal chance (50% in each case) of committing type I and type II errors. Type I error represents the probability of making a false alarm (saying the object is there when actually it is not), and type II error indicates the probability of making a false negative (saying that the object is absent when it is present). The chance classifier would have an EER of 0.5. In this case the lower the EER the better the performance of a classifier. The EER provides additional information by estimating how error prone a classifier is. The AUC only takes into account the chance of

making an error of the first kind, whereas the EER considers both kinds and in consequence provides a complementary picture on the classifier performance. Through this study we use the AUC and EER to discern which network configuration (see section 2.4 for more details) performs better for the task of detecting a prey object.

It is important to mention that this analytical framework has been used before in the context of signal detection in other computational neuroscience problems. For example, Smith and Sherman (2002) have used ROC analyses to study detectability of excitatory and inhibitory drive in an integrate-fire-or-burst neuronal model that mimics thalamocortical relay neurons. In the case of weakly electric fish, the ROC paradigm has been used to assess detection of low frequency stimuli by P electroreceptor afferents (Chacron et al., 2001) and to evaluate feature extraction by bursts of action potentials in ELL pyramidal cells under broadband stimulation *in vivo* and *in vitro* (Oswald et al., 2004).

1.5 Hypothesis and Objectives

Given the importance of the experimental and theoretical results regarding feedback roles as well as the sensory searchlight paradigm introduced earlier, we hypothesize that the direct feedback loop in electrosensory networks will act as an enhancer in the detection of transient signals such as prey. For the present thesis, we have the following objectives and predictions:

- To design two model network scenarios: one in open-loop configuration and the other in closed-loop configuration (i.e. in the absence and presence of neuronal feedback respectively).

- To assess the performance of these networks under a prey-signal detection task, by using ROC analyses. In particular, the role of body-object distance, and strength of feedback inhibitory inputs, will be investigated.
- We predict that under certain conditions (i.e. certain parameters values of the model, see Methods), the closed-loop configuration should perform more reliably than the open-loop one. That is, the AUC's in closed-loop should be higher than those in open-loop; related to this, the EER should be lower in the closed-loop configuration.

Finally, the type of stimuli we used (Gaussian-shaped input currents), and the network architecture we implement, are far more general than for the particular case of the electric fish. As a consequence, this research will shed light on the generalities of feedback effects in the detection of transient signals in other contexts than electrosensory networks. This topic will be addressed in the discussion, where connections with signal detection and prey-capture behaviour will be made more explicit.

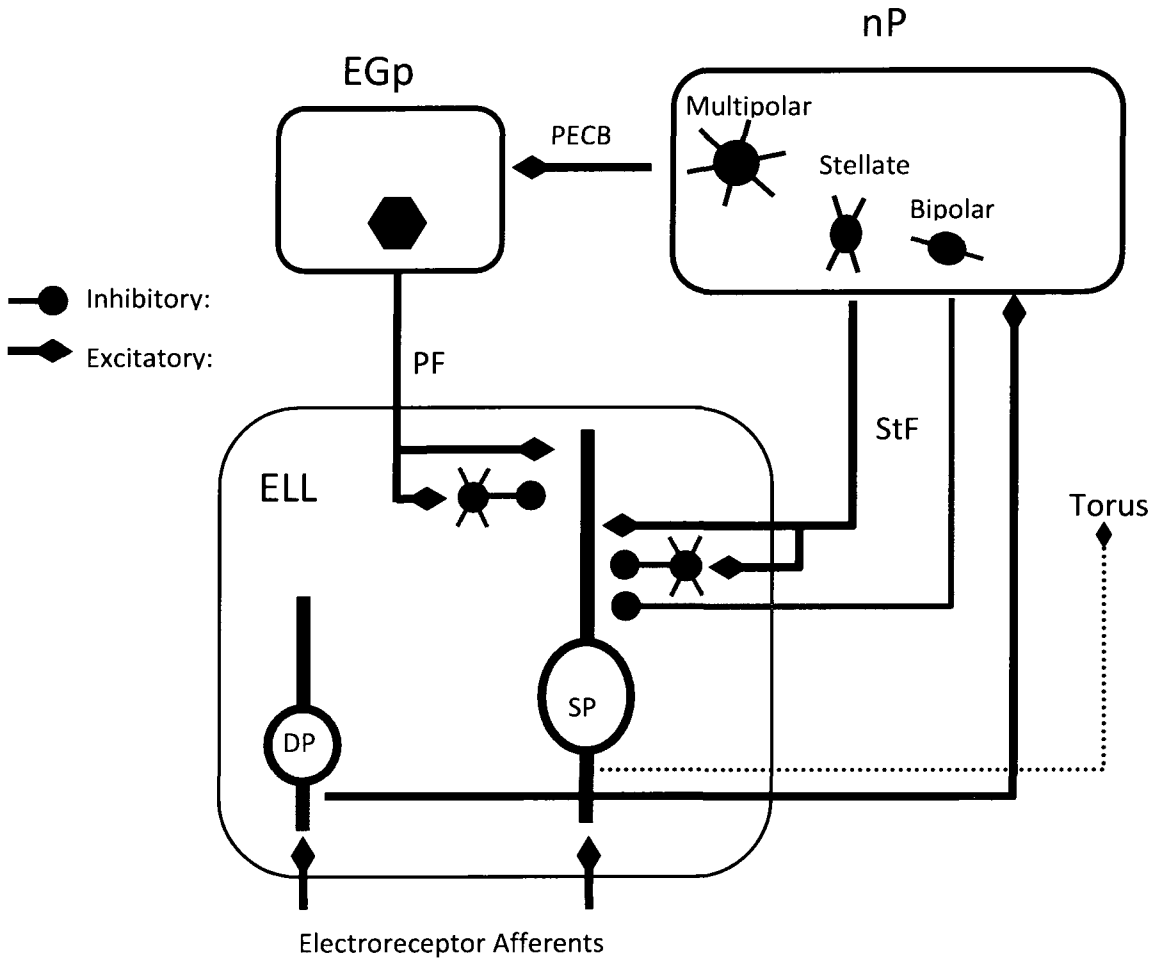

Figure 1.1
Circuitry of the indirect and direct feedback pathways of the electrosensory lateral line lobe (ELL). The nucleus praeminentialis (nP) receives excitatory input primarily from deep pyramidal cells (DP) of the ELL. Superficial pyramidal cells (SP) project primarily to the torus semicircularis (DP neurons also project to torus, not shown). Stellate and bipolar cells of the nP project direct excitatory and inhibitory input respectively, via the tractum stratum fibrosum (StF), onto pyramidal cells of the ELL (both SP and DP subclasses; inputs into DP are omitted for clarity). Stellate cells in nP also activate inhibitory interneurons in ELL which provide disynaptic inhibition onto ELL pyramidal neurons. Multipolar cells of the nP project to the eminentia granularis posterior (EGp) through the praeminential-cerebellar tract (PECB). The granule cells of EGp complete the indirect feedback pathway by projecting parallel fibers (PF) to ELL that mediate excitation and disynaptic inhibition onto ELL pyramidal neurons (inputs into DP neurons are omitted for clarity). Figure modified from Mileva et al. 2008.

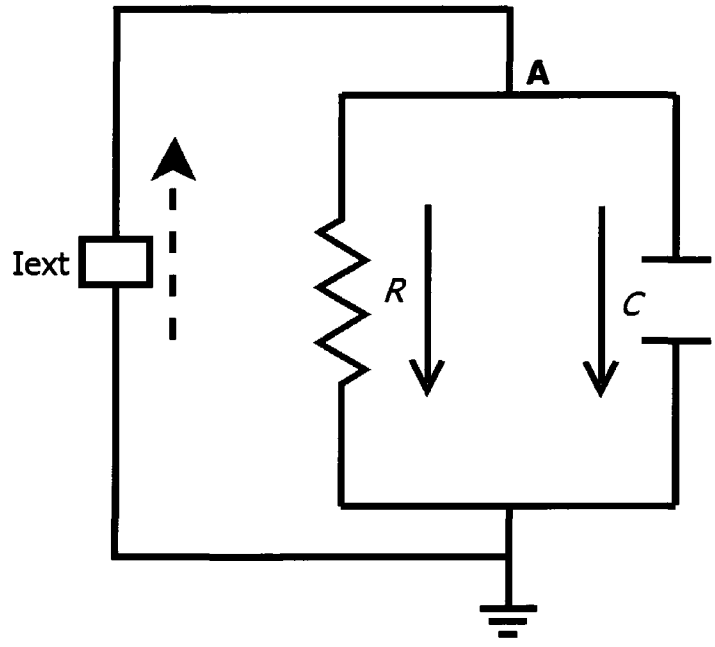

Figure 1.2

Cell membrane equivalent electric circuit. The dynamics of the Leaky integrate and fire model are captured by the resistor (R) and capacitor (C) connected in parallel. I_{ext} is an external current source acting as a stimulus. The flow of currents at node A are schematized by the arrows. The dashed arrow represents the current entering the node (external source), whereas the filled ones represent the current flow through the resistor and capacitor.

i.

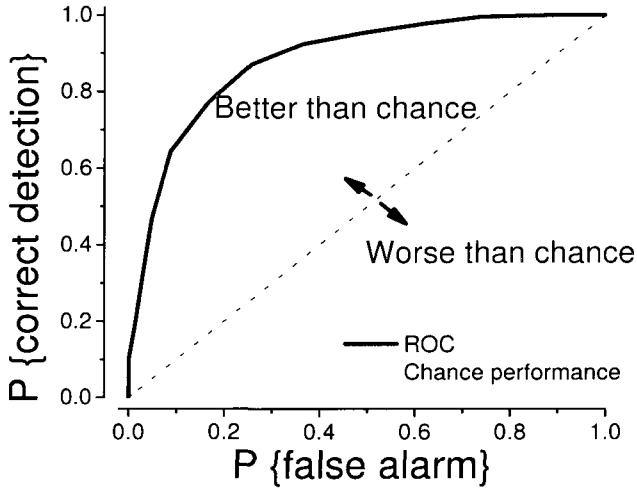

ii.

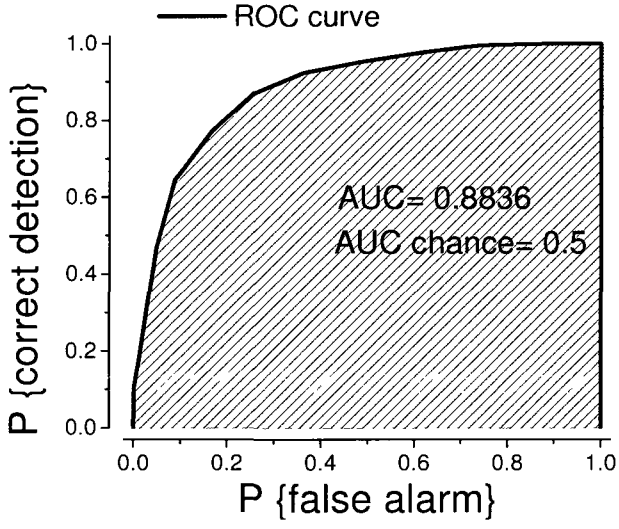

Figure 1.3

i. The receiver operating characteristic curve (ROC). The axes probability of false alarm and probability of correct detection define the ROC space. When an operator is performing a binary classification task, there is a trade-off in between those two probabilities. Points above the principal diagonal represent performances better than a chance classifier, whereas points below the principal diagonal stand for operators that do worse than a chance estimator. **ii.** Example of calculation of the area under the ROC curve (AUC). The greater the AUC the better the performance. A chance classifier has an AUC of 0.5 by definition.

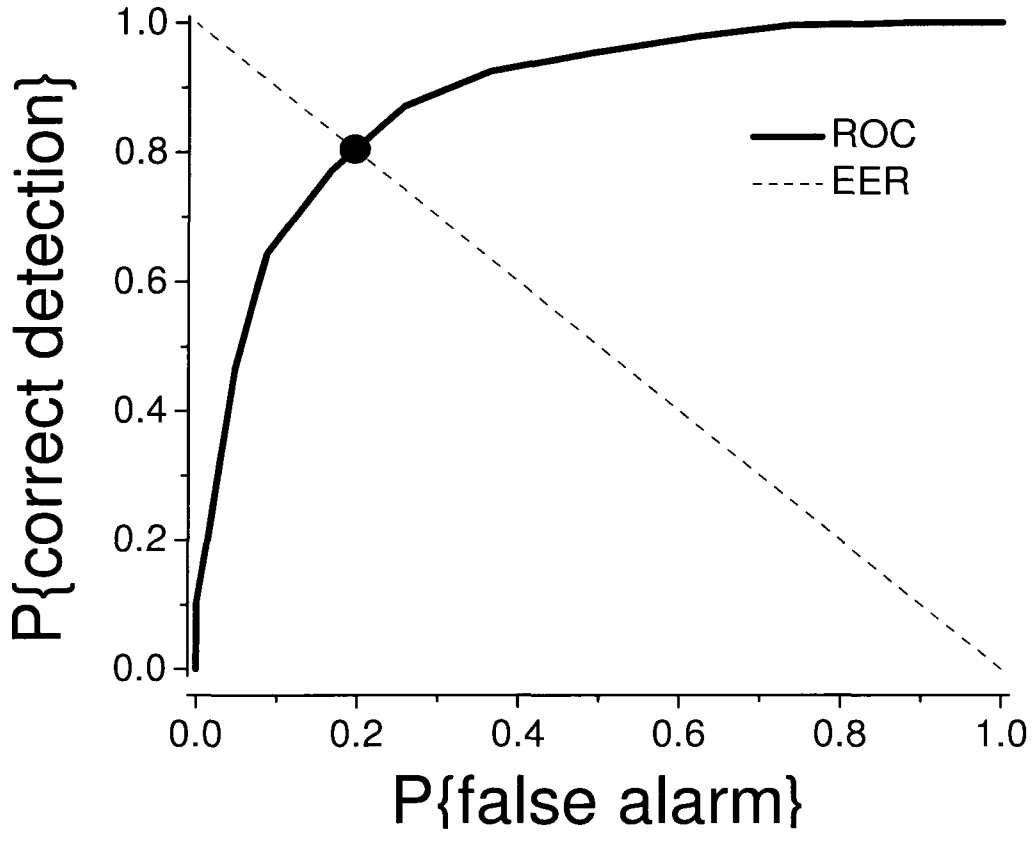

Figure 1.4

The Equal Error Rate (EER) in the Receiver Operating Characteristic (ROC) space.
The EER diagonal represents an observer with 50% chance of committing errors of type I and II. The EER value for the performer is given by the point where the ROC curve intersects with the diagonal. The EER value for the observer is 1 minus the ordinate of that point.

Chapter II

Methods

In the following, we develop a simple modeling approach to study the effects of neuronal feedback on prey detection in the weakly electric fish *Apteronotus leptorhynchus*. Behavioural studies have shown that detection can occur in a single scan of the prey, when the prey is at a distance of around 10mm, but typically not farther than 20mm (Nelson and Maciver, 1999). Therefore, our simulated experiments will consist of a single trial presentation of the prey stimulus, for body-object distances, z_0, chosen among these values: 10, 12, 15 and 20 mm. For generality, we assume that the fish body length is 10 cm and that the scanning velocity is 10 cm s^{-1} based on experimental data available in a closely related species, *Apteronotus albifrons* (Nelson and Maciver, 1999).

2.1 Stimulus input – the electric image

The stimulus current, I_{stim}, represents the input due to a *Daphnia* or similar prey. We used a Gaussian spatial current profile based on an electric image characterization previously made (Lewis and Maler, 2001) given by the following equation

$$I_{stim} = K \times \frac{r_0}{z_0^3} \times e^{\left(-\frac{(x-x_0)^2}{2\sigma}\right)} \tag{2.1}$$

$$\sigma = (c_1 + c_2 \times z_0)^2 \tag{2.2}$$

where K is a stimulus scaling factor, and all other parameters were as previously reported by Lewis and Maler: r_0=0.15cm is the radius of the prey-object, z_0 is the distance from the fish body midline to the center of the *object* (we will further refer to z_0 as the body-object distance), x_0 is the lateral position of the prey (fixed) and the fish scans the object at a constant velocity (10 cm s^{-1}) through the axis of movement x. σ represents the spread of the

electric image, with c_1=-0.055 and c_2=0.79. In this model, the prey is assumed to be a sphere of a given conductivity, an approximation used in previous studies (Babineau et al., 2007; MacIver et al., 2001; Nelson et al., 2002).

Examples of the stimulus set used in the simulations are depicted in Figure 2.1. Each trial consisted of 10 seconds of simulation. The object was placed 5 cm from the fish head when introduced, and the scanning started immediately; due to the spatial extent of the electric image, this resulted in the stimulus being present between t=5 s and t= 6 s.

It is important to notice that this image is at the level of the skin where the P-electroreceptors are located. These electroreceptors convey through afferent fibers trains of action potentials to the pyramidal cells in ELL. It has been experimentally shown that these electroreceptors acts as high-pass filters (Nelson et al., 1997; Xu et al., 1996), and hence are able to encode amplitude modulations such as those produced by prey objects by an increase and subsequent decrease in their basal firing rate. Given this scenario, we assumed that the synaptic current at the pyramidal cell follows the Gaussian shape of the electric image when a prey object is present, with appropriate scaling K (see Results for more details).

The next step is building the neuronal network. We begin by describing its protagonist, the LIF model playing the role of an ELL pyramidal cell.

2.2 Pyramidal neuron model

The pyramidal cell in ELL was modeled as a single compartment LIF unit. Note that we consider an E-type pyramidal cell since they respond to increases in EOD amplitude, and prey-like objects would induce this reaction. This model cell comprises a leakage battery

term, a bias current (I_{bias}), a stimulus current (I_{stim}), and current due to feedback synaptic activity (I_{syn}). The dynamics of the LIF are governed by the following differential equation:

$$\tau_m \frac{dV}{dt} = (V_{leak} - V) + R_m \times [I_{bias} + I_{stim}(t) + I_{syn}(t - \tau_{delay})] \tag{2.3}$$

Each time that V reaches the potential V_{thresh} , an action potential or spike is said to occur, and the variable V is immediately reset to V_{reset} . R_m is the model cell input resistance and τ_m is the membrane time constant. τ_{delay} stands for the temporal delay to receive feedback inputs. Equation (2.3) was solved using a forward Euler integration scheme with time-step Δt (Press et al., 1992). Values of these parameters, as well as all other equation parameters presented in this chapter, can be found in Table 2.1.

A refractory period in the LIF model was omitted since our choice of parameters set the firing rate in the transition zone of no firing and low-frequency firing (i.e. well below saturation). Therefore, inclusion of a refractory period in this regime will not have an effect on the intrinsic dynamics of the circuit.

In the following section, feedback connectivity is added to this basic building block.

2.3 Feedback models: Open and closed loop

The synaptic current modelling differs for the open and closed network scenarios (Figure 2.2). In the open loop case, this synaptic activity is uncorrelated from the stimulus and independent of the LIF activity (Figure 2.2.i). The overall firing rate of this feedback pathway is fixed and is given by the following expression:

$$R = N_f \times 16 \tag{2.4}$$

Where N_f represents the number of fibers providing synaptic input to the LIF compartment, each one firing at 16 Hz.

This rate, R, both in open and closed loop cases drives a monosynaptic excitatory process and a disynaptic inhibitory process dependent of the rate of excitation (Figure 2.2). These processes were modeled as stochastic conductances activated in time as a Poisson processes with rate R. It is important to remark that in the closed loop context the Poisson processes are rate modulated (see later).

The implementation is as follows; first we computed the excitatory events. If the following expression,

$$\alpha \times R \times \Delta t > U_1 \tag{2.5}$$

was true; where U_1 is a random number chosen from uniform distribution in the interval 0 to 1, α is the excitatory gain, R is the rate of excitation and Δt is the integration time-step, then the total excitatory conductance (G_{exc}) was increased with this update rule:

$$G_{exc}(t) = G_{exc}(t - \Delta t) + g_{exc} \tag{2.6}$$

where g_{exc} is the unitary excitatory conductance.

If the expression (2,5) was false, then the total excitatory conductance decayed towards 0, governed by a first-order differential equation:

$$\frac{dG_{exc}}{dt} = \frac{-G_{exc}}{\tau_{exc}} \tag{2.7}$$

As previously stated the rate of inhibition (R_{inh}) was dependent on the rate of excitation through disynaptic connections (see Fig 2.2). We modelled this dependency with a first-order differential equation:

$$\frac{dR_{inh}}{dt} = \frac{\beta \times R - R_{inh}}{\tau_{Rinh}} \tag{2.8}$$

where β is the inhibitory gain and R the rate of excitation. This expression allows the inhibitory rate to grow with increasing excitatory input up to a limit value set by the inhibitory process itself. With this rate (R_{inh}), again a conductance model is used with the same logic as for the excitation. If the expression,

$$R_{inh} \times \Delta t > U_2 \tag{2.9}$$

holds true, where U_2 is again a random number chosen form a uniform distribution ranging from 0 to 1, then the total inhibitory conductance (G_{inh}) was updated in this way:

$$G_{inh}(t) = G_{inh}(t - \Delta t) + g_{inh} \tag{2.10}$$

where g_{inh} is the unitary excitatory conductance. If expression (2.9) was false then the total inhibitory conductance decayed exponentially to zero in this fashion:

$$\frac{dG_{inh}}{dt} = \frac{-G_{inh}}{\tau_{inh}} \tag{2.11}$$

Lastly the synaptic current is given by:

$$I_{syn}(t) = G_{exc}(t) \times (V_{exc} - V(t)) + G_{inh}(t) \times (V_{inh} - V(t)) \tag{2.12}$$

where V_{exc} and V_{inh} are the reversal potentials for the excitatory and inhibitory currents respectively.

This type of implementation for the synaptic current has been previously used to study the dynamics of the indirect feedback pathway and its implications in negative image cancellation (Lewis et al., 2007).

In the closed loop situation, the synaptic current due to feedback is dependent on the level of activity in the LIF model cell (Figure 2.2.ii). To account for this effect we have to estimate the LIF instantaneous firing rate (F). In order to do this the spike times of the LIF were used to compute on-line a binary sequence of events with time resolution Δt that we refer to as the spike train.

The instantaneous firing rate, the number of spikes produced per unit time, was estimated by combining a first-order low-pass filtering of the spike train with an instantaneous discrete update rule in the case a spike was produced (Dayan and Abbott, 2001). The implementation is in the following way:

$$\begin{aligned} &\text{if } V(t) \geq V_{thresh} \\ &\quad F(t) = F(t-\Delta t) + \tau_F{}^{-1} \end{aligned} \tag{2.13}$$

In other words, each time an action potential occurs, the estimate of the firing rate (F) is increased by a finite amount $\tau_F{}^{-1}$. At all other times, F decays exponentially to zero with time constant τ_F :

$$\frac{dF}{dt} = \frac{-F}{\tau_F} \tag{2.14}$$

With the time dependent firing rate ($F(t)$) we proceed to calculate the rate of activity of the feedback nucleus in the following way:

$$R = N_f \times F(t) \tag{2.15}$$

The total delay due to feedback in the direct feedback pathway has been experimentally measured, and estimated to be 12 msec (Doiron et al., 2003). In equation (2.3) this delay (parameter τ_{delay}) is taking into account when delivering synaptic current inputs in the closed loop configuration.

2.4 Evaluating and quantifying model performance

We define three time windows, A, B and C each of length 500msec. The window A comprises the 500 msec prior to stimulus onset, B is centered at the peak of the Gaussian distribution representing the stimulus (Figure 2.1), and C is the window just following window B (Figure 2.3). In this way we ensure that for the broadest stimulation (20 mm, Figure 2.1), the whole stimulus dynamics is included in time window B.

In each time window, we computed the number of spikes (or action potentials) produced during that period, i.e. the spike counts. Each experimental condition was simulated 1000 times in order to compute spike count distributions and reliable statistics on them. The spike counts were binned with 1 spike/bin resolution from 0 to counts bigger than 20, and histogram calculations were performed. An example of these distributions can be seen in figure 2.4. The mean and standard deviations of these distributions where calculated to compare them with experimental values (see section 2.5).

These distributions were used to establish performance analyses to compare prey detection in open and closed loop. Comparisons were made using the Receiver operating characteristic (ROC) paradigm (Fawcett, 2006; Green and Swets, 1966). In this context two spike count distributions are defined: one when the prey is absent ($p_0(n)$) and the other when the prey is present ($p_1(n)$), where n is the spike count. An ideal observer counting j spikes in a time window would be able to tell the probability of making a correct detection (P_D) or making a false call/alarm (P_{FA}). The ROC curve is computed by varying the threshold value j across the interval, $-\infty \leq j \geq +\infty$, and by plotting the pairs (P_{FA}, P_D) for each value of j. The expressions for P_{FA} and P_D are as follows:

$$P_{FA} = \sum_{n \geq j} p_0(n) \tag{2.16}$$

$$P_D = \sum_{n \geq j} p_1(n) \tag{2.17}$$

The area under the ROC curve (AUC) is one of the most reliable measurements of performance (Bradley, 1997; Cortes and Mohri, 2004; Hand and Till, 2001; Jin et al.; Ling et al., 2003), and is defined in this way:

$$AUC = \int_0^1 ROC \, dP_{FA} \tag{2.18}$$

This area was numerically computed by trapezoidal integration of the points defining the curve (Fawcett, 2006). Interestingly, the AUC is equivalent to performing a U Mann-Whitney test (Bamber, 1975; Hanley and McNeil, 1982):

$$AUC = \frac{U_{MW}}{n_1 \times n_2} \tag{2.19}$$

where n_1 and n_2 are the sample sizes (1000 for both samples in the present study). For large sample sizes (n > 30) the U Mann-Whitney statistic is normally distributed (Mann and Whitney, 1947; Wilcoxon, 1945) . Therefore it is possible to use a z-test to see if an AUC value is different from the chance classifier (AUC=0.5). In our case the standard error (S.E.) for the AUC is 0.0127 for all simulations in accordance with Hanley and McNeil (1982). We therefore calculated the 95% lower and upper confidence intervals for the chance classifier, which are 0.475 and 0.525 respectively. Values outside this interval are considered statistically significant at the 5% level.. Confidence limits for the chance classifier are included as a dashed box in the figures presented.

Another common measure to compare detectors or classifiers is the equal error rate (EER). In this case, it is assumed that the observer will commit Type-I and Type-II errors with equal probabilities. As a reminder the Type-I error is equivalent to the P_{FA}, and the Type-II error is equivalent to $1-P_D$, and is also referred to as the probability of a false negative. The EER is then defined as the minimum error an observer can make under those circumstances, and it is calculated in the following way:

$$EER = \min(0.5\times(P_{FA}+1-P_D)) \tag{2.20}$$

As opposed to the AUC, the smaller the EER the better the performance.

In order to further compare the performance between open and closed loop configurations, we developed a new measurement that we called the response contrast, which is very similar in nature to a paired test such as the Wilcoxon Sign Rank Test (Wilcoxon, 1945). The first step is to compute two new distributions: the first one is the subtraction of spike counts in time window B with time window A (B-A) on a trial by trial basis; the second one is to perform a subtraction of spike counts between time windows B and C (B-C) also on a trial to trial basis. In this way, we are comparing the signal/stimulus against the pre and post stimulation respectively. We have taken the B-A distribution as the null, and the B-C as the alternative. Then using these two new distributions we performed ROC analysis and computed AUC's and EER's as before. For the AUC, the comparison is equivalent to using a non parametric paired test as the Wilcoxon Sign Rank Test (Sheskin, 2000; Wilcoxon, 1945), and again for large sample sizes this statistic is normally distributed.

All other results were considered statistically significant if $p<0.05$.

2.5 Testing the model in the absence of stimulation

Making fair comparisons between the different network scenarios requires that the mean firing rates in the absence of stimulation should be similar. In addition, we decided to match this baseline firing with the experimental values recorded both *in vivo* and *in vitro* in the pyramidal cells of the ELL nucleus of *Apteronotus leptorhynchus*, which are approximately 15 Hz (Oswald et al., 2004). We proceeded to tune the model parameters to establish the desired baseline. We achieve this by using as a starting point the parameter values reported by Lewis and collaborators (2007). Then we proceed to remove the spiking mechanism and check that the variations in membrane voltage were in the fluctuation-driven regime (Kuhn et al., 2004). This is that sufficient amount of stochastic variation was seen both in the excitatory and inhibitory directions. Then, we replaced the spiking mechanism and conducted final adjustments in parameters to get similar firing responses in open and closed loop.

For the set of parameters reported (Table 2.1), the medians of the spike counts distributions in open and closed loop configurations did not differ statistically (Mann-Whitney U Test, $p=0.4116$), in the absence of stimulation and were in close agreement with the experimental values (open loop: mean=14.5 Hz, SD= 3.6 Hz; closed loop: 15.1 Hz, SD=5.9 Hz). However, the null (i.e. without stimulation) distributions in open and closed loop were not normally distributed (Lilliefors Test, $p<0.001$) and these distributions were statistically different (χ^2 test, $p<0.001$). This is due to the fact that in closed-loop the spike count distributions tend to be broader. An example of this can be seen in Figure 2.4. In addition, the differences in the distributions can be attributed to some burstiness in the closed-loop configuration.

It is important to notice that the behaviour of the model and the agreement with experimental values does not depend exactly on the parameter values reported here. We varied most of the parameters by ±20% of the reported values in Table 2.1, without noticing any qualitative or quantitative changes in the model response. Therefore, we decided to report the midpoints of those intervals, which are the values used in the simulations presented in this thesis unless otherwise stated.

2.6 Equipment and software used

All simulations and data analysis were performed on a PC computer running MATLAB 7.0.4 (Mathworks, Natick, MA, USA).

Table 2.1 Parameter values for all the equations presented in the methods chapter.

parameter	value
R_m	10 MΩ
τ_m	12 msec
I_{bias}	0.5 nA
τ_{delay}	12 msec
V_{leak}	-70 mV
V_{thresh}	-65 mV
V_{reset}	-70 mV
τ_F	300 msec
Δt	0.1 msec
N_f	30
α	1
g_{exc}	5.6×10^{-3} S
τ_{exc}	5 msec
β	1, 2, 4
τ_{Rinh}	100 msec
g_{inh}	$\frac{600\times10^{-4}}{\beta\times4.5}$ S
τ_{inh}	10 msec
V_{exc}	0 mV
V_{inh}	-80 mV

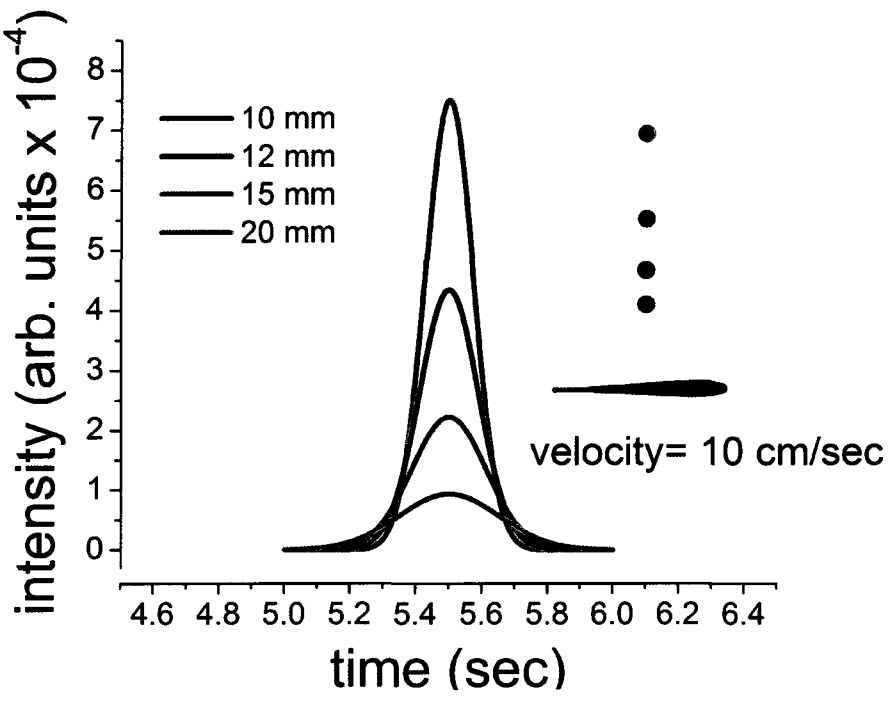

Figure 2.1 Stimulus set used to mimic used to mimic prey.

The stimuli used are one-dimensional Gaussian current profiles. The change in amplitude (arbitrary units) is described for body-object distances of 10, 12, 15 and 20 mm respectively. The x-axis is in units of time, we converted the spatial Gaussian profile into the temporal domain by using linear interpolation in the time-step Δt, assuming that the fish is scanning the object once at a constant velocity of 10 cm s^{-1} (fish body length=10 cm). The object is presented once in each round of simulation.

i.

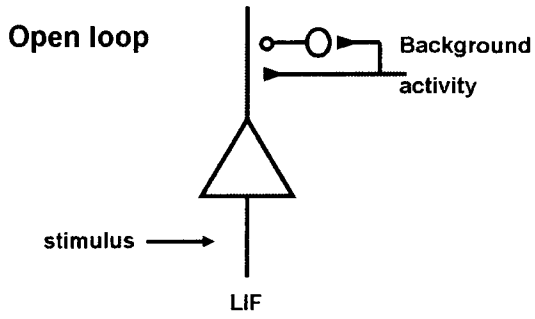

ii.

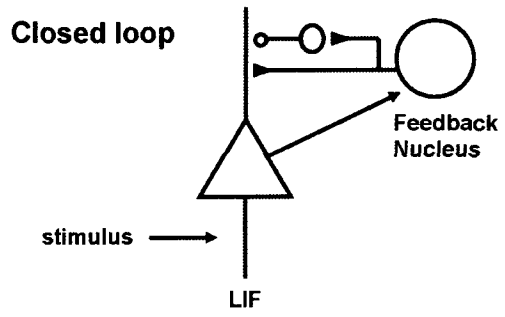

Figure 2.2 Open and closed loop network configurations.

i. Open loop: the stimulus is presented to the LIF. Background synaptic activity is presented in the form of monosynaptic excitation and disynaptic inhibition. This activity is uncorrelated of the stimulus and LIF firing response. In the open loop configuration, the rate of the background synaptic activity is fixed. Excitation and inhibition conductances are modelled as Poisson processes. **ii.** Closed loop: the stimulus is presented to the LIF. The feedback nucleus estimates the firing of the LIF. This rate is used to drive inhibitory and excitatory processes with the same architecture than in open loop. In this case the levels of inhibition and excitation are rate-modulated and dependent on the LIF activity. Conductances are hence rate-modulated Poisson processes. After a fixed delay a synaptic current product of the feedback is introduced to the LIF compartment.

i.

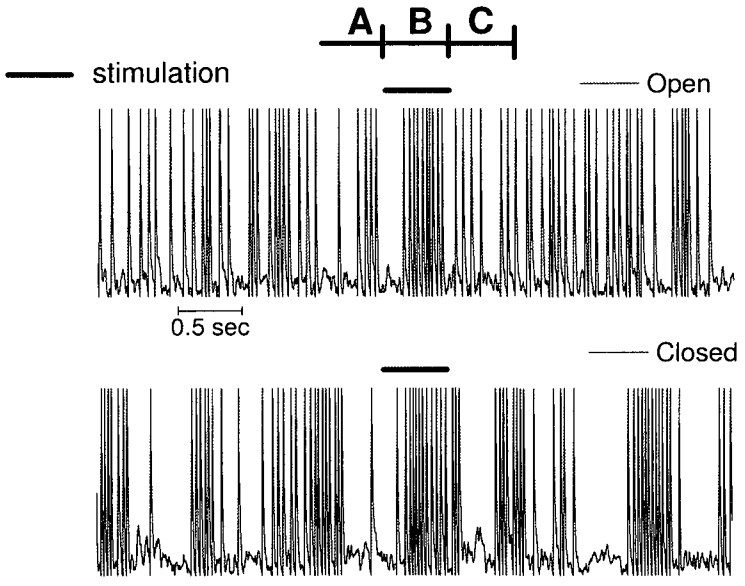

ii.

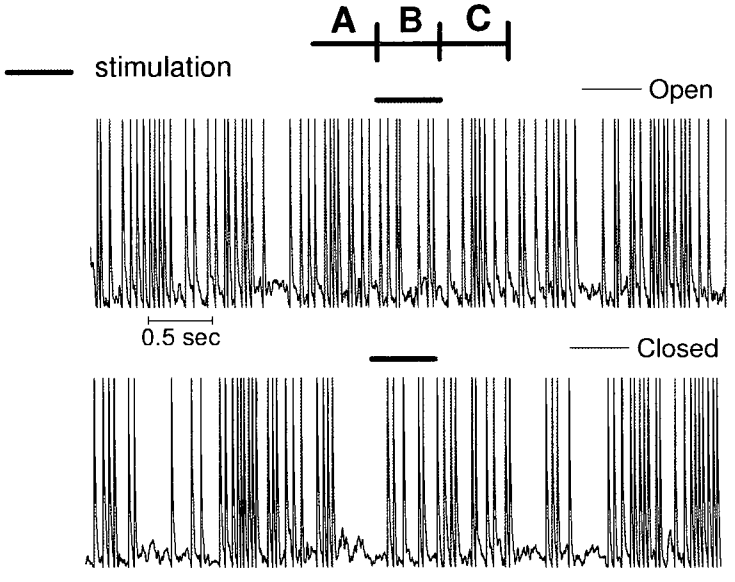

Figure 2.3 LIF activities in open and closed loop configurations.
Sample voltage traces of the LIF compartment, showing spiking activity. The object was placed at 10mm (**i.**) and at 20 mm (**ii.**) from the fish body. Spike counts were computed during adjacent time windows A, B, C each one of 500 msec duration. Time window B is centered at the peak of the Gaussian current mimicking the prey. Therefore Time window A is the pre-stimulation, and Time window C the post-stimulation.

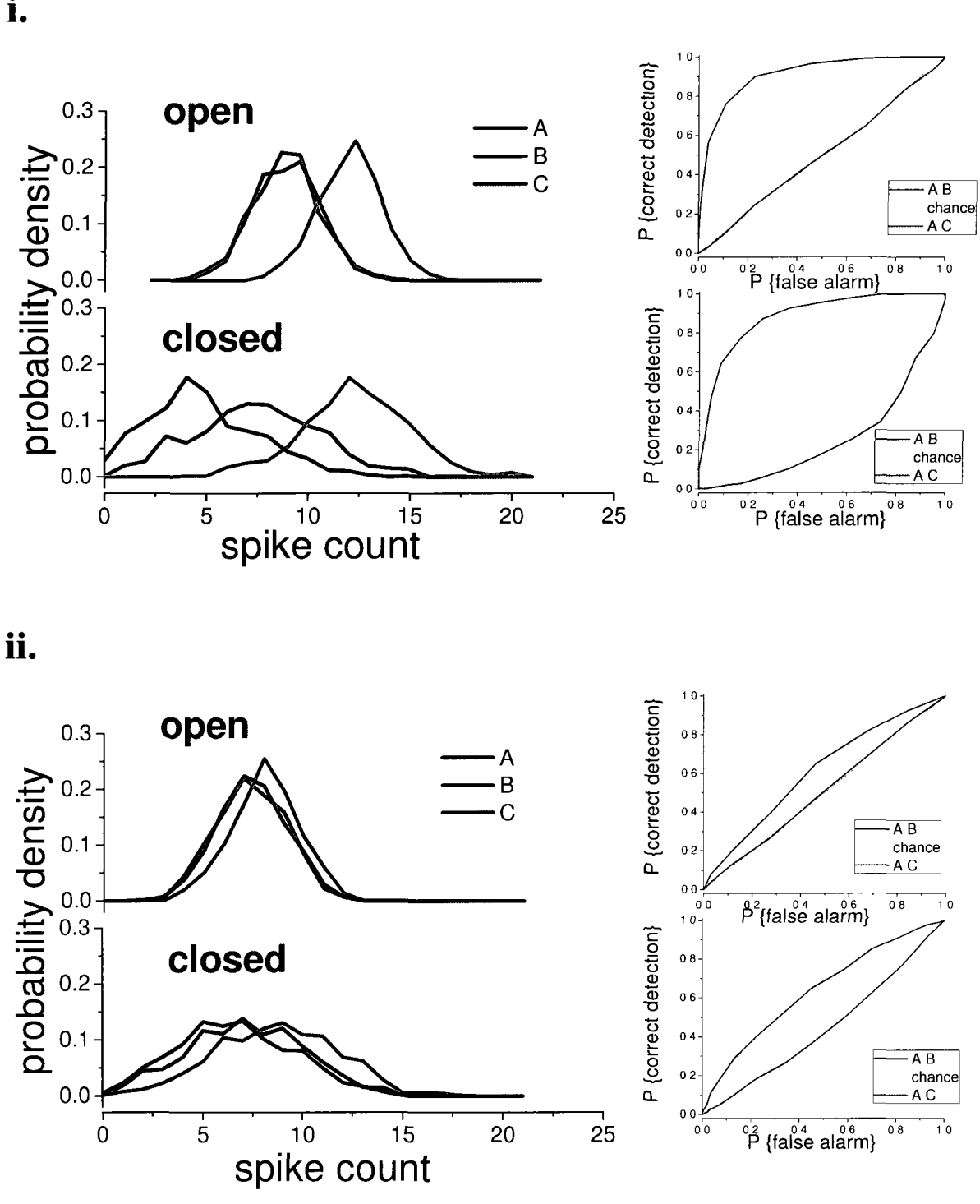

Figure 2.4 Spike counts distributions for time windows A, B and C in open and closed loop. **i**. Histograms calculated for a 1000 realizations of simulations with object at 10 mm from the fish body. **ii.** Same as **i.** but body-object distance is 20 mm.
Insets are the corresponding ROC curves.

Chapter III

Results

3.1 Setting the baseline conditions: adjusting stimulus scaling factor

Experimental characterization of ELL pyramidal cell responses to different stimuli has been previously done (Bastian, 1986). However, the type of stimulus used (a 9 mm metal cylinder) hinders any direct comparison with objects mimicking prey such as *Daphnia* or worms. Typical preys have radii of ~1.5 mm and much lower conductivity than metals (Nelson et al., 2002). More recently, another set of studies (Maler, 2009a; 2009b) has theoretically characterized the receptive field of ELL pyramidal cells in the three topographic maps: centromedial, centrolateral and lateral segments (CMS, CLS and LS respectively). In addition, the response of these receptive fields to objects mimicking prey (almost identical stimulus implementation) has been characterized across maps. Maler chose to compute spike counts over a 200 msec time window in order to perform Fisher information analyses on the estimation of prey location. Our choice of time window is longer (500 msec) to account for the full duration of the prey stimulus during scanning, but we have chosen a stimulus scaling factor that produced similar responses (in terms of firing rate) to those reported by Maler (2009b). Figure 3.1 reports the effects of the stimulus scaling described above on detectability when the body-object distance is the shortest (10 mm). The AUC increases monotonically with stimulus scaling K when comparing time windows A and B, for both open and closed loop network configurations (Figure 3.1.i). In addition, the AUC's for time windows A and B are statistically different than chance level (z-test) for both open and closed loop configurations. Nonetheless, for A and B time windows, closed and open loop performances are very similar. Differences in response are 3% in the largest case. However, the situation is different when comparing time windows A and C (Figure 3.1.ii). In this case we are comparing the pre and post stimulation, taking A as the null distribution. In the open

loop scenario, the AUC's for all K values do not differ significantly from chance levels (z-test). But, in the closed loop context all, AUC's values are significantly lower than chance levels (z-test). The fact that the AUC's are below 0.5 reflects that the distribution associated with time window C is shifted to the left of the one associated with time window A.
For the following results sections we have chosen a stimulus scaling factor of 0.005, as it gives the biggest response that is still comparable with Maler's previous studies.

3.2 The effect of body-object distance in the detection response

As seen in figure 2.1, the amplitude and shape of the stimuli varies greatly with body-object distance. For the shortest body-object distance (10 mm) the peak amplitude is maximal for the stimulus set used and the spread is minimal. As the body-object distance z_0 is increased, the peak of the signal decreases and the spread increases. Given the nature of the stimulus set, we wanted to explore the effects of varying z_0, in the relevant biological interval, on object detection performance for the two network scenarios studied.

For stimulus detection at time windows A and B, the general trend is that AUC's for both open and closed loop decline monotonically with increasing body-object distance (Figure 3.2.i). Here again, both open and closed loop in time windows A and B are statistically different from chance levels for all distances (z-test). But, performance in closed and open loop in the A and B time windows are very similar (largest difference is 3% in AUC). However, for pre and post stimulation time windows (A and C respectively), open loop configuration AUC's are not different from a chance classifier for all values of body-object distances (z-test), while closed loop performance is always significantly below chance levels (z-test), and the AUC increases with increasing body object distance (Figure 3.2.ii).

Again, this is because the spike count distribution in time window C is shifted to the left of the one pertaining to the A time window. This observation, that we find also in the following sections, has led us to develop another measure (the response contrast, see Methods section 2.4), to account in a more robust fashion for the silent phase in the post stimulation period (indicated by the leftward shift of the spike-count distribution).

In figure 3.3 we present the effects of body object-distance on the response contrast. The idea is to assess the probability of making a misclassification in both directions, i.e. either making a false negative or a false positive. This is equivalent to measuring statistical errors of the first and second kind.

In the open loop scenario the performance cannot be distinguished on a statistical basis from a chance classifier (z-test). Noticeably, in the closed loop configuration all AUC's are bigger and statistically different than 0.5 (z-test). Interestingly, the AUC for the response contrast in closed loop declines with increasing body-object distance.

The next logical step was to assess the Equal Error Rate using the response contrast. In figure 3.4 it is shown that EER values for the open loop network are approximately 0.5 for all distances tested, and hence the chance to make a mistake is comparable to the error rate of a chance classifier. Additionally, we found that the EER in closed loop is minimal (0.36) when the object is closest to the body, and increases monotonically as the object moves further away from the body, reaching a maximum error rate of 0.47. At the furthest distance the error rates in open and closed loop are thus comparable in magnitude.

3.3 Assessing the role of feedback: inhibition and its contributions to detection

The main objective of this thesis is to establish the role of neuronal feedback in object detection. In the preceding section we showed that feedback can improve detection performance under the assumptions of an ideal observer. In this section, we want to understand how the balance between excitatory and inhibitory feedback affects this behaviour. We decided to perform a test for the model at the closest body-object distance (i.e. 10 mm). Varying the strength of the excitatory processes, by increasing or decreasing its gain, did not produce any qualitative nor quantitative change in the overall response of the model (data not shown). Remarkably, this was not the case for the inhibitory processes. The increase in performance and detection abilities in the closed loop configuration was highly dependent on the strength of the inhibition controlled by the gain factor (β, eq. 8). In the next paragraph we explore the effect of changing the inhibitory gain while keeping the excitation fixed.

In figure 3.5, model performances when inhibition strength is varied are depicted. When comparing time windows A and B, three important trends are observed (Figure 3.5.i). First, the AUC values for open and closed loop network scenarios are statistically different from a chance classifier (z-test). Second, the AUC values are high for both configurations (averaging 0.90 in both cases) and the inhibitory gain does not affect the AUC values (maximal dispersion from the mean value is 0.03 units). Third, there are no noticeable differences for open and closed loop in this case. Nonetheless, when comparing the pre and post stimulation (i.e. time windows A and C) the trends are very different. In the first place, the open loop network performance cannot be distinguished from a chance classifier at the considered significance level (z-test) for all values if inhibitory gain used. Secondly, the

closed loop configuration produced AUC values below 0.5 (and statistically different from chance, z-test), with AUC values declining with increasing inhibitory strength (Figure 3.5.ii).

As previously mentioned this is due to a left-shift of the spike count distributions during time window C compared to those of time window A. To clarify the situation we again use response contrast as a measure (figure 3.6). The AUC's for the open loop configuration are again indistinguishable on statistical grounds from a performer that guesses if the object is there or not, with a probability of saying yes equal to 0.5 (and hence the negation probability is 0.5 as well). But, the response of the closed loop network is of a different nature. To begin with, all AUC's values in closed loop are higher and statistically different than 0.5 (z-test). Additionally, AUC increases monotonically with inhibitory gain, reaching a maximum of 0.71 when the inhibitory gain is 4. However, this performance increase does not continue indefinitely. Indeed, if the inhibitory gain is increased over 4, regular bursting starts to occur, even in the absence of stimulation. Autonomous bursting, in this case is detrimental to stimulus detection and will result in a subsequent decrease in AUC to chance levels (and underperforming open-loop in most circumstances). This situation will be addressed in more depth in the Discussion chapter.

For the response contrast we also measured the equal error rate. In figure 3.7 we can see that the EER for open loop is approximately 0.5 for all values of inhibitory gain. Hence there is no difference in the level of error committed when compared to a chance classifier. In the case of the closed loop configuration the EER declines systematically with increased inhibitory gain, reaching a minimum of 0.33 when the inhibitory gain is 4.

3.4 The effect of τ_{Rinh} on feedback dynamics

We also investigated the role of τ_{Rinh}, the time constant governing the differential equation that relates the rate of excitation with the inhibition rate, on how it affects feedback dynamics and consequently network performance in object detection.

For values of τ_{Rinh} ranging from 10 msec to a 100 msec (the value finally used, see Table 2.1) the behaviour of the model and thus the performance in detection didn't change in any significant way (Figure 3.8).

A valuable inference from these results and the one presented in the previous section, is that the behaviour of the closed loop dynamics are much more sensitive to variations in the strength of the inhibitory gain than to changes in one order of magnitude in τ_{Rinh}. In spite of this, when τ_{Rinh} was increased beyond a 100 msec, the dynamics of the network changed suddenly. In closed loop particularly, bursting was very intense and regular even in the absence of any stimulation. As mentioned in the preceding section, this bursting is problematic for the detection of transient signals.

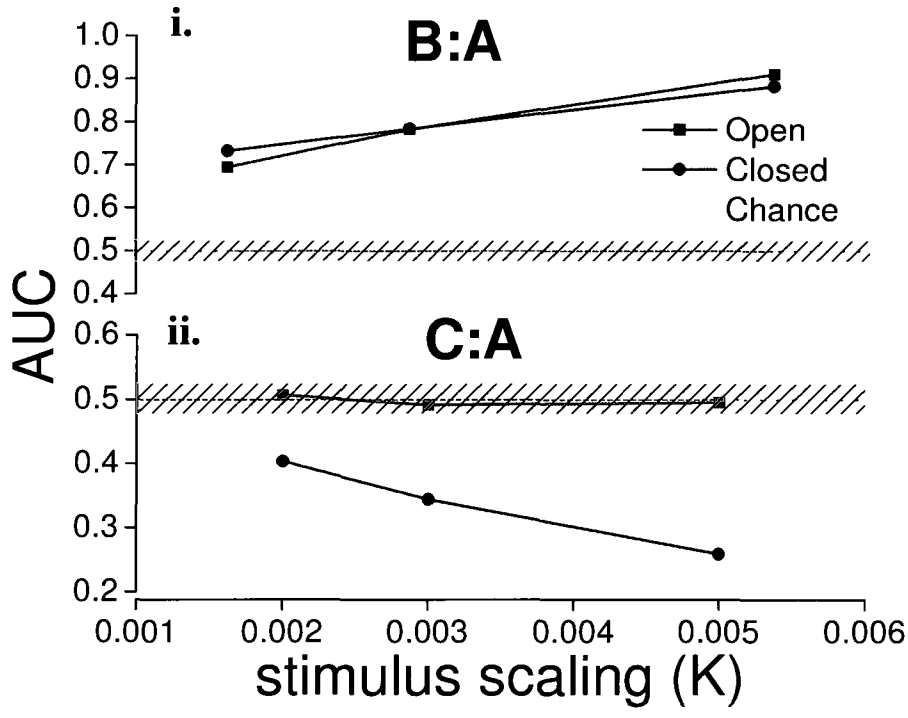

Figure 3.1 Effects of stimulus scaling on performance reported as changes in AUC. 1000 realizations of each condition were calculated to compute spike count distributions and perform ROC analyses. The AUC's for time windows A vs. B (prior to stimulation and during stimulation) for open and closed loop network configurations are presented in panel **i.** In panel **ii.** AUC's for prior vs. post stimulation (time windows A and C) are presented. Dashed line represents the performance by a chance classifier, and 95% confidence limits are indicated as a diagonal shadowing. Parameter β was set to 2, and z_0 was set to 10 mm.

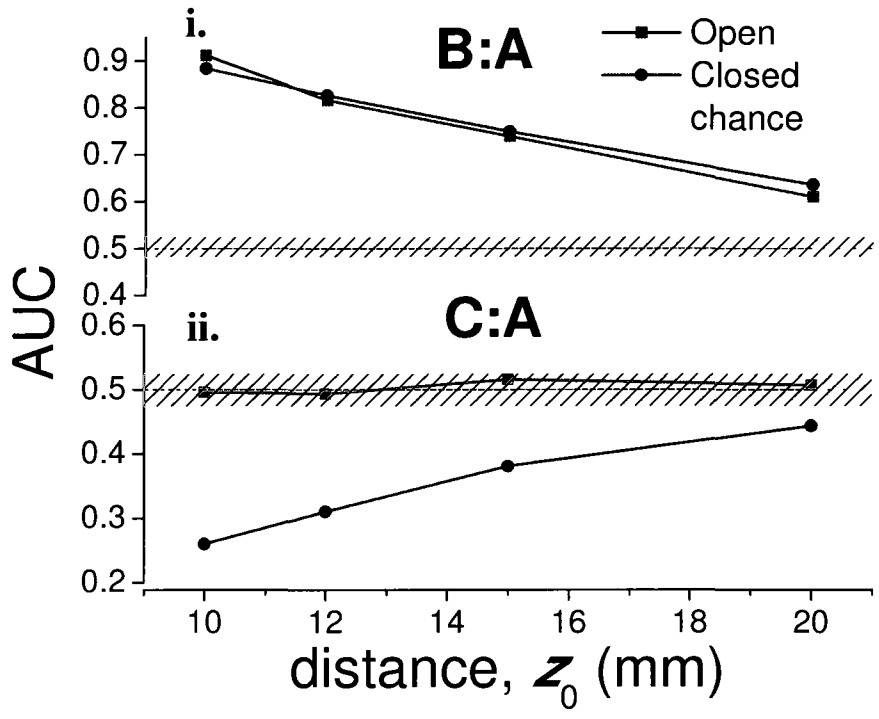

Figure 3.2 Effect of body-object distance on signal detection measured as AUC.

i. AUC's for open and closed loop using spike distributions for time windows A and B, when body-object distances were 10, 12, 15 and 20 mm. **ii.** Same as **i.** but for pre and post stimulation (Time windows A and C respectively).
Dashed line represents the performance by a chance classifier and includes a diagonal shadowing pattern for the 95% confidence limit.
AUC Calculations were based on a 1000 realizations on each condition for both panels.
Parameter β was set to 2.

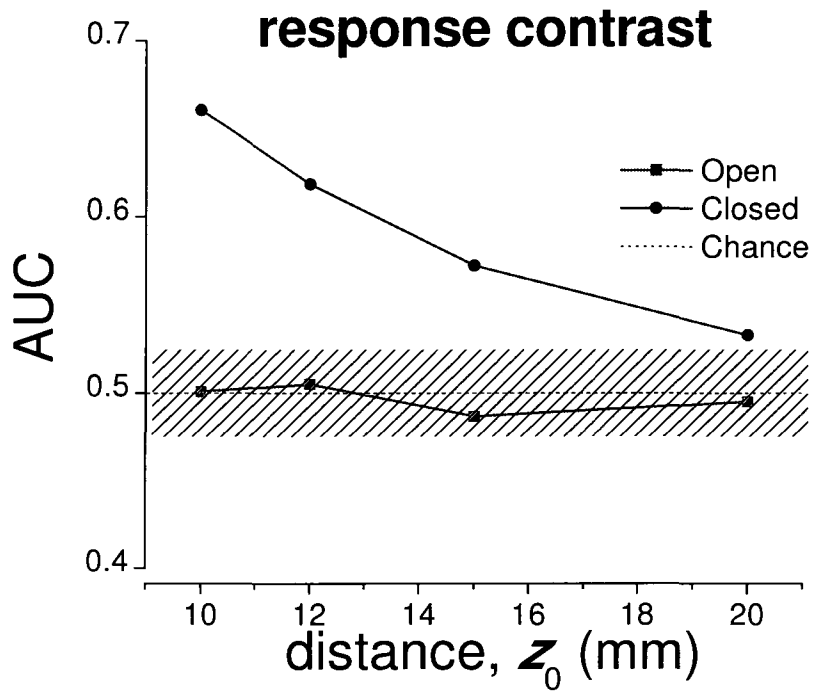

Figure 3.3 AUC for the response contrast measurement when body-object distance was varied.
ROC analyses were performed for the distributions time windows B-A and B-C, defined as the response contrast. Changes in AUC as a function of the body-object distance are reported, for both open and closed loop scenarios. Dashed line represents the performance by a chance classifier and includes 95% confidence limits as a diagonal shadowing pattern. AUC Calculations were based on a 1000 realizations on each condition. Parameter β was set to 2.

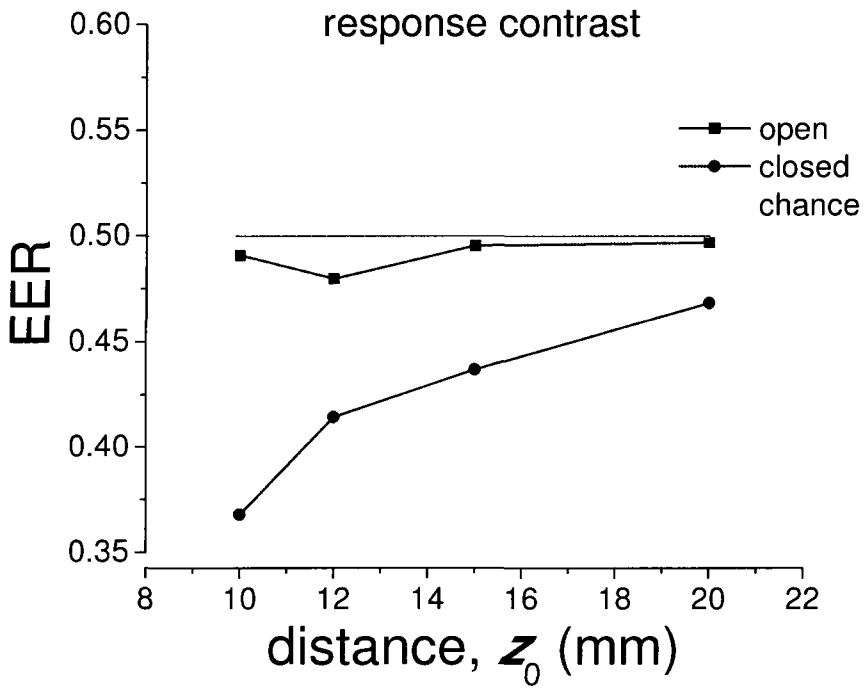

Figure 3.4
Equal error rates for the response contrast as function of the body-object distance. The performance by a chance classifier is included as a dashed line. EER Calculations were based on a 1000 realizations on each condition, with parameter β set at 2.

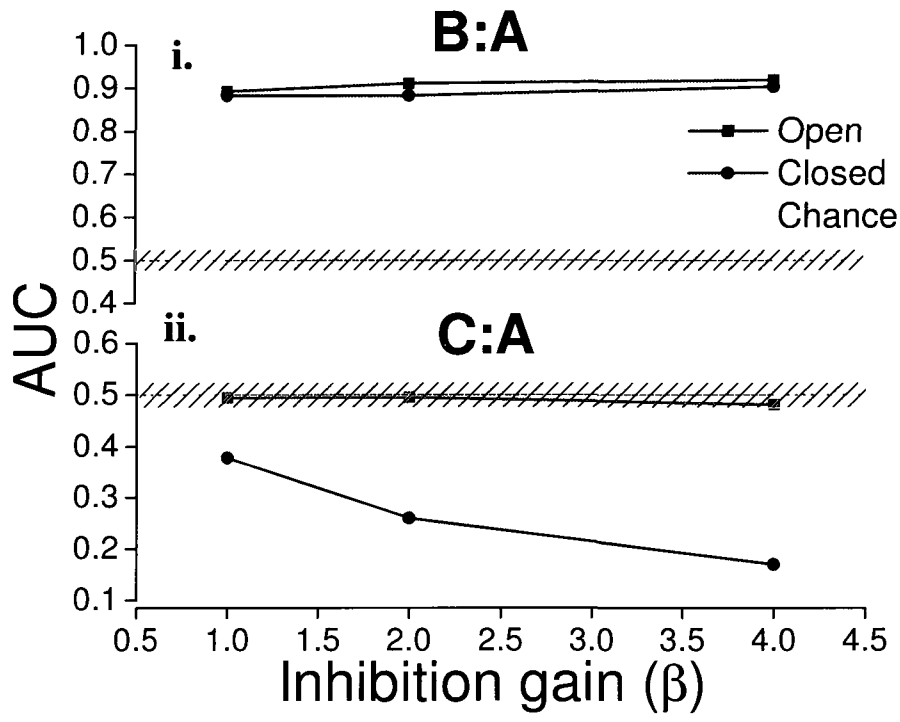

Figure 3.5 Effect of feedback inhibitory inputs on prey detection reported as changes in AUC.
In panel **i.** AUC's comparing time windows A and B as a function of the inhibitory gain are presented, for both open and closed loop networks. **ii.** Same as **i.** when comparing pre and post stimulation (time windows A and C respectively).
Dashed line represents the performance by a chance classifier and includes 95% confidence limits as a diagonal shadowing pattern. AUC calculations were based on a 1000 realizations on each condition. Parameter z_0 was set to 10 mm.

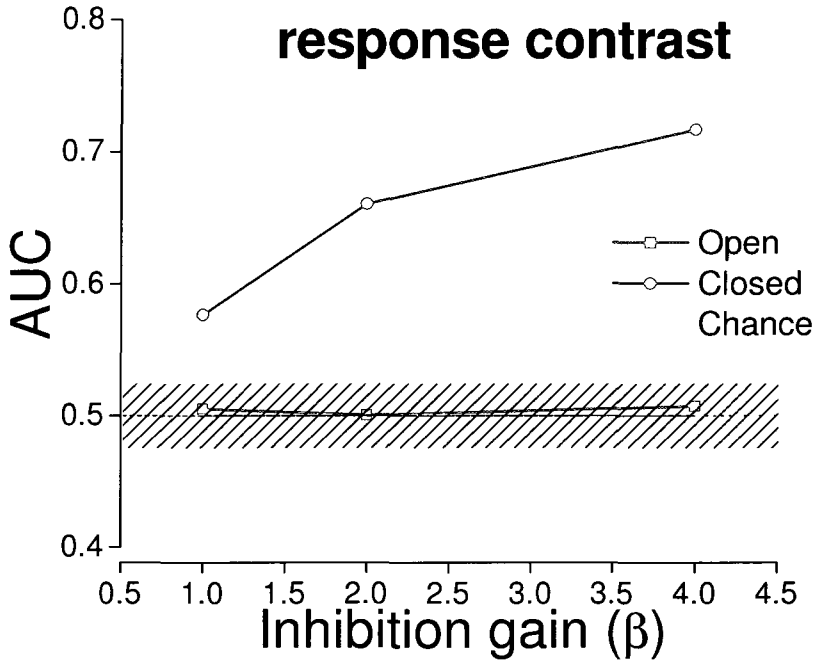

Figure 3.6 Changes in AUC for the response contrast measurement, when feedback inhibitory input gain is varied.
ROC analyses were performed for the distributions time windows B-A and B-C, defined as the response contrast. Dashed line represents the performance by a chance classifier and includes 95% confidence limits as a diagonal shadowing pattern. AUC calculations were based on 1000 realizations on each condition. Parameter z_0 was set to 10 mm.

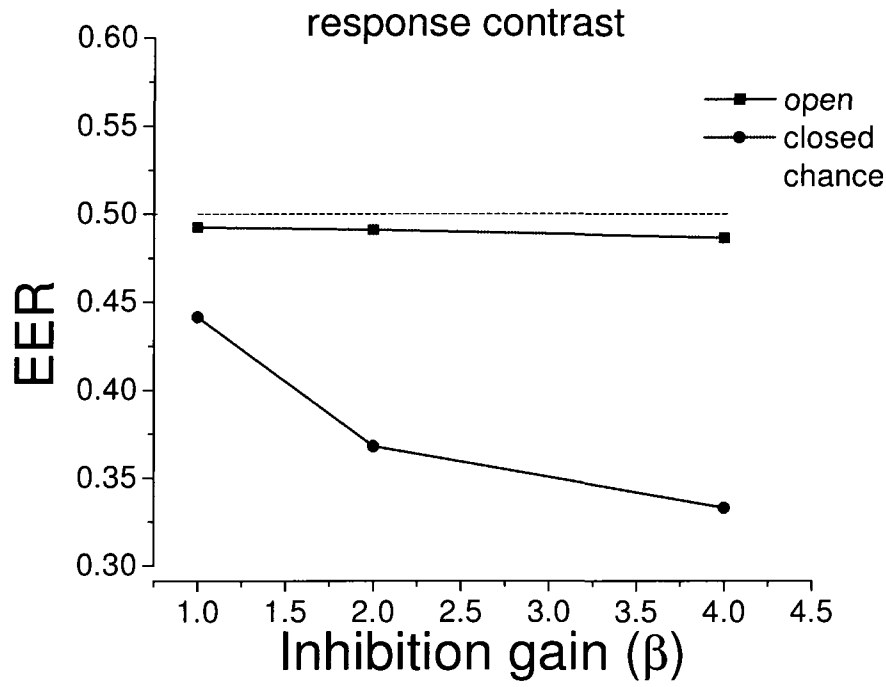

Figure 3.7 Equal error rates for the response contrast as function of feedback inhibitory input strength.
The performance by a chance classifier is included as a dashed line. EER calculations were based on 1000 realizations on each condition, with parameter z_0 set at 10 mm.

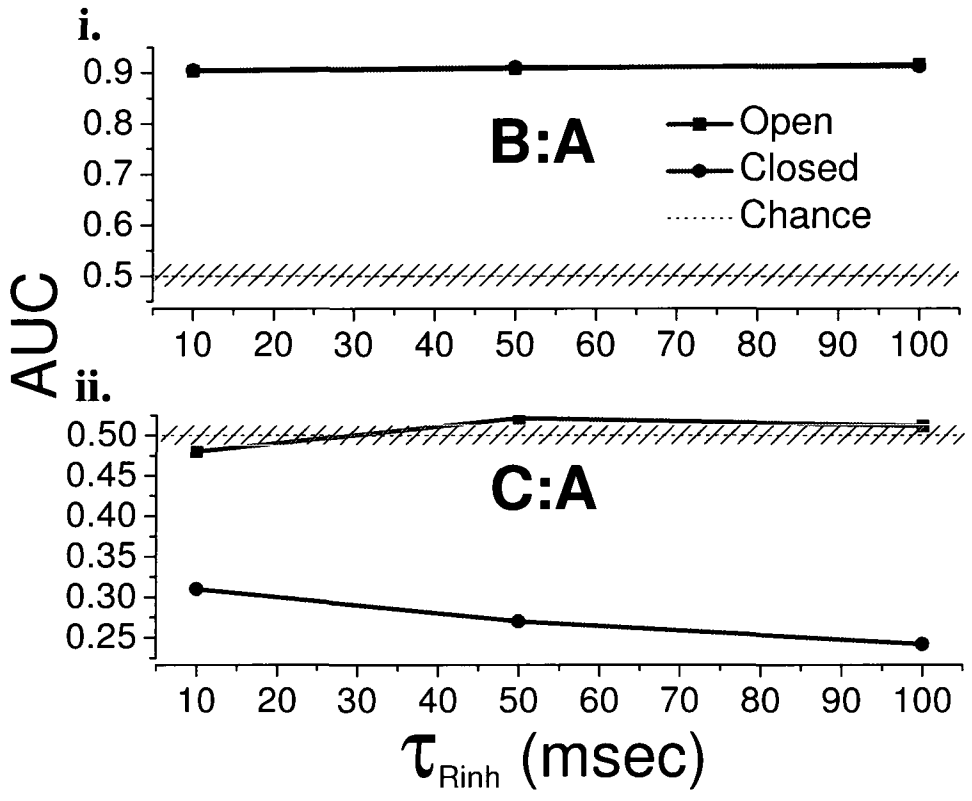

Figure 3.8 Effect of the rate of inhibition time constant (τ_{Rinh}) on feedback dynamics evaluated as changes in AUC.
i. Comparison of time windows A and B and ii. comparison of time windows A and C. Dashed line represents the performance by a chance classifier and includes 95% confidence limits as a diagonal shadowing pattern. AUC calculations were based on 1000 realizations on each condition. Parameter z_0 was set to 10 mm, and parameter β was set to 2.

Chapter IV

Discussion

4.1 Feedback as an enhancer of weak and transient signals

Feeding is one of the basic and prototypical behaviours characterizing animal life. Therefore, it is relevant to ask how an animal detects prey in order to satisfy one of its basic needs. This is particularly interesting when the sensory signal due to prey is low in amplitude and transient in its spatial-temporal extension, and is as a consequence difficult to detect. We want to understand how the neuronal circuits responsible for sensory processing achieve this difficult task, by focussing our attention on the role of feedback in transient signal detection. In the present study, we introduced a model circuit that mimics an early stage of the electrosensory network of the weakly electric fish *Apteronotus leptorhynchus*. We tested the response of this model to stimuli that represent prey under two different feedback configurations, open-loop and closed-loop. In figures 3.3 and 3.4 we reported that the closed-loop configuration performs better in detecting prey presented in a single trial, when the body-object distance is varied, as compared to the open-loop network. Under a ROC curve analysis paradigm, this increased performance is indicated by a higher AUC and lower EER. These results support the hypothesis that feedback can enhance the detection of prey in a certain distance range. However, when the body-object distance is large (20 mm) the performance almost drops to levels comparable to a chance classifier. This is comparable to previous results coming from a model evaluating prey distance estimation (Maler, 2009b). In Maler (2009b), the neuronal network is aiming to estimate the body-object distance (i.e. object localization), whereas in our case we are concerned about detection, i.e. having a statistical criteria to say if the prey is there or not. Maler reported that for distances above 30 mm the network he implemented can no longer estimate the body-object distance. It is important to note that both, Maler's and our results, are in agreement with previous

theoretical (Ludtke and Nelson, 2006) and experimental (Gussin et al., 2007) studies showing that for body-distances above ~25 mm, the firing rate modulations of P-units are below noise levels, and hence detection by pyramidal cells will be compromised (Maler, 2009b). Nonetheless, this is the first study to our knowledge showing the effects of feedback on signal detection applied to the electrosensory network. The results showed in this thesis provide further support to the hypothesis that the direct feedback pathway acts as a sensory searchlight (Crick, 1984) enhancing the detection of weak and transient signals.

In spite of this, the specific architecture of our network in closed-loop does not reflect all the detail of the real biological network. In our closed-loop model we linked the LIF neuron (i.e pyramidal cell) with projections to a feedback nucleus playing the role of nP. Then this feedback core sends feedback inputs to the same cell that was originally stimulated. This is an assumption that the topography of the feedback is reciprocal (Berman and Maler 1999). However, experimental work suggests that most of projections to nP arise from deep pyramidal cells, and that most of the feedback projections (at least those showing synaptic plasticity) synapse onto superficial pyramidal cells (Bastian and Bratton, 1990; Bastian et al., 2004). In other words, the projection neurons are different from those receiving the feedback. Instead, we are assuming a single neuron plays both roles, a simplification based on the recently-described columnar organization of the ELL (Maler, 2009a). That said, preliminary work (data not shown) on a model comprising a more realistic electrosensory network topology shows results similar to those we report for the simplified network.

Our simplified network also resembles prototypical feedback loops found in other sensory systems (e.g. vision, olfaction and audition in vertebrates), as well as in cerebellar and cortical-thalamic pathways. In all of these cases, the detection of weak and transient

signals can be important. Therefore, having basic and general model connectivity might help to understand other relevant problems in neuroscience. It would be interesting to extend the analysis on signal detection to other types of transient stimuli with different temporal profiles, in addition to the Gaussian tested in the current study. In these cases we predict that if the signal is transient and not widely spread in the temporal domain, it can be amplified by our network in closed-loop, without caring much about the exact details. Regarding stimulation, we are assuming that the LIF neuron follows the stimulus input (P-afferents activity) in a linear fashion. Under these circumstances, we assumed that the synaptic current at the pyramidal cell also follows a Gaussian shape of the electric image when a prey object is present, with appropriate scaling K (Figure 3.1). This is true for deep pyramidal cells in ELL (Chacron, 2006), but not for superficial pyramidal cells.

4.2 The precise role of feedback: importance of inhibition

The next logical step was to provide insight on how feedback influenced prey detection in the 10 to 20 mm body-object distance range. In our first explorations of the model we kept the excitatory and inhibitory feedback inputs balanced in terms of the gain. In other words, if excitatory rate increased, inhibition was increased such that no net change in LIF membrane potential would occur (this is the "balanced condition"). Under this condition, prey detection did not differ in open and closed loop (data not shown). Additionally, we explored the response of the model when the feedback inputs were unbalanced (conditions reported in this thesis). When excitation gain was higher than the inhibitory gain ($\beta=1, \alpha<6$), the performance of the open and closed loop configurations were very similar in terms of AUC and EER (data not shown); and in some cases where excitation was very

strong ($\alpha > 6$) the open-loop network outperformed the closed-loop configuration. These observations led us to explore the role of inhibitory feedback inputs on prey detection. In figures 3.5, 3.6, and 3.7 we analyze the model performance in prey detection, as the gain of the inhibitory feedback input is varied. It is important to note that the feedback pathways in ELL have been shown to exhibit various forms of synaptic plasticity (Bastian et al., 2004; Lewis and Maler, 2002; Oswald et al., 2002) and thus the relative gain of excitation and inhibition can be considered a dynamic variable under natural conditions. In summary, the detection of the prey is better in closed loop as the inhibitory feedback inputs get stronger. However, it is important to mention that if the inhibitory gain goes beyond 4, bursting starts to occur. The same is true if the time constant controlling the dynamics of the inhibitory feedback activation (τ_{Rinh}) goes over a 100 msec. Autonomous bursting is detrimental for any neural coding scheme based on spike counts and ROC analyses. This is because the bursts of spontaneous activity can be confused with the transient signal leading to an increased probability of false positives being detected. This will depend on the timing of the stimulus delivery relative to the bursting phase. It would be interesting to further explore this possibility by probing the object repeatedly at different bursting phases to see if there are any dependencies that affect prey detection. Regardless, such bursting must be distinguished from transient bursts that can actually enhance coding and even code for specific features of a stimulus (e.g. Oswald et al., 2004)

In another context, bursting in electrosensory networks has been implied as a switch to distinguish two network states - oscillatory and non-oscillatory – that are associated with communication signals (chirps) and local, low frequency signals such as prey, respectively (Doiron et al., 2003). In other animal systems, neuronal network oscillations have been shown to code odorant signals, which can be considered multidimensional objects (Laurent,

2002). In addition, the topology of the olfactory bulb network is very similar to the columnar organization we are using in the present study.

Getting back to the coding problem, if bursting occurs, other choices for extracting information from the spike train might be available. One possibility is to use a temporal code (Theunissen and Miller, 1995); this considers the variations in the spike time series, rather than how many spikes are produced in a fixed time window. Here, we can explore correlations in the inter-spike interval sequence, and determine if these correlations increase or decrease when the prey is present. In this case, the decision rule would be based on the value of those correlation coefficients. Again, a ROC paradigm can be used to calculate detection performance based on the distributions of those correlation coefficients, under different circumstances. This type of coding could also apply to cases where the signal (in terms of spike rate) is below noise levels as discussed earlier, even though it has been suggested that experimental testing of this possibility might be easier to perform in pulse type fish rather than in wave type weakly electric fish (Maler, 2009b). Nonetheless, experimental evidence of temporal coding exists in the rat somatosensory barrel cortex involved in the whisking system (Ahissar and Knutsen, 2008; Knutsen et al., 2008; Petersen et al., 2002). Rats use repetitive movement of their whiskers to locate objects, and in this system inhibitory feedback is also important to perform this task in an efficient and effective way (Knutsen and Ahissar, 2009).

4.3 Main findings and the broader context

In the present thesis we have shown that feedback dependent enhancement of weak and transient signals is constrained to the matching of these two requirements:

- A delayed inhibition with respect of excitation
- An inhibition that has a stronger gain than the excitation.

These conditions allow to amplify and enhance transient and weak signals. The process is two-fold. In the first instance, when the stimulus appears there is an increase in activity (reported as spike counts). At this time, excitatory processes lead the response with little contribution from the inhibitory inputs. However, as the stimulus vanishes there is an interplay in between the duration of the stimulus and the delay for inhibition to kick in. If these time scales have appropriate and sufficient overlap, at the end of the stimulation and for a short period after it, there is a decrease in spiking activity compared to the basal level (prior to stimulation). At this time, inhibition is dominating and excitation plays a secondary role. This biphasic response, i.e. transient increase in spike count followed by a decrease compared to control levels, due to closed-loop dynamics is the core mechanism underlying the more robust detection of transient signals when closed-loop feedback is present. The development of the response contrast measurement (see section 2.4) was based on this noticeable biphasic response. However, we need to find a biophysical explanation for a decoding mechanism: that is, how the subtraction of the two distributions can be calculated on a biological basis. It is important to recall that differentiation in the temporal domain is equivalent to applying a high-pass filter (mathematically both involve the same operation). Given this fact and experimental evidence that P-afferent encode AM of the EOD acting as high-pass filters (Nelson et al., 1997; Xu et al., 1996), one possible explanation is that the differentiation occurs at the level of the P-afferents (i.e. presynaptically to the pyramidal cells in ELL). Also, at the level of the P-afferents spike frequency adaptation -another differentiation mechanism- occurs for transient communication signals such as chirps (Benda

et al., 2005) and hence a similar mechanism for prey transient signals can contribute to give physiological grounds to the response contrast measurement we have developed. Additionally, P-afferents are affected by fast short term synaptic plasticity leading to noise reduction (Khanbabaie et al., 2010), and previous theoretical studies have shown that this type of dynamics can lead to differentiation (Abbott and Regehr, 2004; Ludtke and Nelson, 2006). Also, differentiation can occur at the level of pyramidal cells in ELL. The plausibility of this mechanism remains to be studied at the experimental level to finely dissect the ionic currents that might be responsible for such a mathematical operation to occur. All these differentiation mechanisms are taking place and occurring before any feedback inputs are added to the system. Therefore, they are expected to contribute to detection enhancement regardless of feedback configuration. But, for decoding to occur and for understanding the precise role of feedback, we must think of processes that take place upstream of ELL. In this regard, short-term depression is involved in gain control mechanisms (Abbott et al., 1997). Even more, short-term depression has been recently described in the ELL-torus semicircularis synapse, as being responsible for the extraction of complex stimulus features that ELL by itself cannot decode (Chacron et al., 2009). Therefore, it is possible that the torus is acting as a higher level decoder in terms of the problem of prey detection. The underlying operational mechanism might be based on a short-term depression affecting feedback gain, allowing for the subtraction of the spike counts involved in the response contrast, and hence being able to detect and decode the presence of a prey.

From the preceding discussion, it seems like the direct feedback pathway of the electrosensory network may require an optimal balance of inhibition and excitation. Improper amounts of excitation or inhibition, as well as the time scales of these processes, would lead to poor performances on one hand, or to conditions where the activity in open

and closed loop can not be distinguished on the other. However, from the results reported using a statistical technique based on the ideal observer paradigm, it is clear that when the feedback is properly tuned it helps to perform a detection task by providing additional information in the post stimulation period. It would be interesting to further investigate which physiological mechanisms provide stability to the conditions required for the feedback to be fully operational in regards of prey detection. Stability is important and central because prey detection is linked to a basic behaviour, feeding.

The results of this work can be further interpreted in a neuroethological context; this is linking the basic neural mechanisms that make possible fundamental behaviours for the survival of the organism. An additional step in this direction would be to interpret the role of neural feedback for prey detection under the framework of the optimal foraging theory. This ecological theory aims to understand how foragers invest their resources – time and energy- allocating them in an optimal fashion, by minimizing their investment (Stephens et al., 2007; Stephens and Krebs, 1986). Given that our results suggest that feedback acts as a sensory searchlight enhancing prey objects, it would be interesting to analyze how feedback helps to minimize time and energy expenditure for these fish to forage in their natural habitats. A final remark in regards to the optimal foraging theory is that most modelling in this context is based on an ideal observer paradigm, and ROC analyses are common to assess forager selection on different prey patches (e.g. Rechten et al., 1983). Therefore, it is interesting to make connections to a particular behaviour at all levels of description particularly when there is a commonality in the analytical techniques being used.

Finally, the main result presented in this thesis, that closed-loop feedback improves the detection of weak and transient signals under certain conditions, can be extended to other systems besides the electrosensory system because the network architecture we have

assumed is common in neural systems. We believe that this is one of the strengths of our model. The other important fact regarding this simple network model is that its validity can be tested experimentally, by constructing so-called hybrid networks. This is the interface of real neurons and networks with artificial/model networks in real-time (Arsiero et al., 2007; Prinz et al., 2004; Sharp et al., 1993a; Sharp et al., 1993b). This technique would allow for example a pyramidal neuron in an ELL slice preparation to be connected with a model mimicking feedback inputs (Lewis et al., 2007; Mileva et al., 2008). Such experiments could directly test our model on real neurons and give a more robust and precise answer to the question of how feedback operates to enhance transient and weak signals in the electrosensory network, and in neuronal networks in general.

¿Qué es la vida? Un frenesí.

¿Qué es la vida? Una ficción,

una sombra, una ilusión,

y el mayor bien es pequeño.

¡Que toda la vida es sueño,

y los sueños, sueños son!

Pedro Calderón de la Barca
La vida es sueño

Bibliography

Abbott, L. F. (1999). Lapicque's introduction of the integrate-and-fire model neuron (1907). *Brain Research Bulletin* **50**, 303-4.

Abbott, L. F. and Regehr, W. G. (2004). Synaptic computation. *Nature* **431**, 796-803.

Abbott, L. F., Varela, J. A., Sen, K. and Nelson, S. B. (1997). Synaptic Depression and Cortical Gain Control. *Science* **275**, 221-224.

Agmon, A. and Connors, B. W. (1992). Correlation between intrinsic firing patterns and thalamocortical synaptic responses of neurons in mouse barrel cortex. *Journal of Neuroscience* **12**, 319-29.

Ahissar, E. and Kleinfeld, D. (2003). Closed-loop Neuronal Computations: Focus on Vibrissa Somatosensation in Rat. *Cerebral Cortex* **13**, 53-62.

Ahissar, E. and Knutsen, P. M. (2008). Object localization with whiskers. *Biological Cybernetics* **98**, 449-58.

Arsiero, M., Lüscher, H. R. and Giugliano, M. (2007). Real-time Closed-loop Electrophysiology: towards new frontiers in in vitro investigations in the Neurosciences. *Archives Italiennes de Biologie* **145**, 193-209.

Babineau, D., Lewis, J. E. and Longtin, A. (2007). Spatial Acuity and Prey Detection in Weakly Electric Fish. *PLoS Computational Biology* **3**, e38.

Bamber, D. (1975). The area above the ordinal dominance graph and the area below the receiver operating characteristic graph. *Journal of Mathematical Psychology* **12**, 387-415.

Bastian, J. (1986). Gain control in the electrosensory system mediated by descending inputs to the electrosensory lateral line lobe. *Journal of Neuroscience* **6**, 553-62.

Bastian, J. (1994). Electrosensory organisms. *Physics Today* **47**, 30-37.

Bastian, J. (1995). Pyramidal-cell plasticity in weakly electric fish: A mechanism for attenuating responses to reafferent electrosensory inputs. *Journal of Comparative Physiology. A, Sensory, Neural, and Behavioral Physiology* **176**, 63-78.

Bastian, J. (1996). Plasticity in an electrosensory system. I. General features of a dynamic sensory filter. *Journal of Neurophysiology* **76**, 2483-2496.

Bastian, J. (1999). Plasticity of feedback inputs in the apteronotid electrosensory system. *Journal of Experimental Biology* **202**, 1327-1337.

Bastian, J. and Bratton, B. (1990). Descending control of electroreception. I. Properties of nucleus praeeminentialis neurons projecting indirectly to the electrosensory lateral line lobe. *Journal of Neuroscience* **10**, 1226-1240.

Bastian, J., Chacron, M. J. and Maler, L. (2004). Plastic and Nonplastic Pyramidal Cells Perform Unique Roles in a Network Capable of Adaptive Redundancy Reduction. *Neuron* **41**, 767-779.

Bell, C. and Maler, L. (2005). Central Neuroanatomy of Electrosensory Systems in Fish. In *Electroreception*, eds. T. H. Bullock C. D. Hopkins A. N. Popper and R. A. Fay, pp. 68-111. New York, USA. Springer.

Benda, J., Longtin, A. and Maler, L. (2005). Spike-frequency adaptation separates transient communication signals from background oscillations. *Journal of Neuroscience* **25**, 2312-21.

Berman, N. J. and Maler, L. (1999). Neural architecture of the electrosensory lateral line lobe: adaptations for coincidence detection, a sensory searchlight and frequency-dependent adaptive filtering. *Journal of Experimental Biology* **202**, 1243-1253.

Bradley, A. P. (1997). The use of the area under the ROC curve in the evaluation of machine learning algorithms. *Pattern Recognition* **30**, 1145-1159.

Bratton, B. and Bastian, J. (1990). Descending control of electro-reception. II. Properties of nucleus praeeminentialis neurons projecting directly to the electrosensory lateral line lobe. *Journal of Neuroscience* **10**, 1241-1253.

Brunel, N. and van Rossum, M. C. (2007). Lapicque's 1907 paper: from frogs to integrate-and-fire. *Biological Cybernetics* **97**, 337-9.

Carr, C. E., Maler, L. and Sas, E. (1982). Peripheral organization and central projections of the electrosensory nerves in gymnotiform fish. *Journal of Comparative Neurology* **211**, 139-153.

Chacron, M. J. (2006). Nonlinear information processing in a model sensory system. *Journal of Neurophysiology* **95**, 2933-46.

Chacron, M. J., Longtin, A. and Maler, L. (2001). Negative Interspike Interval Correlations Increase the Neuronal Capacity for Encoding Time-Dependent Stimuli. *Journal of Neuroscience* **21**, 5328-5343.

Chacron, M. J., Longtin, A. and Maler, L. (2005). Delayed excitatory and inhibitory feedback shape neural information transmission. *Physical Review E* **72**, 051917.

Chacron, M. J., Toporikova, N. and Fortune, E. S. (2009). Differences in the Time Course of Short-Term Depression Across Receptive Fields Are Correlated With Directional Selectivity in Electrosensory Neurons. *Journal of Neurophysiology* **102**, 3270-3279.

Cortes, C. and Mohri, M. (2004). AUC Optimization vs. Error Rate Minimization. In *Advances in Neural Information Processing Systems 16*, eds. S. Thrun L. Saul and B. Schölkopf. Cambridge, Massachusetts. MIT Press.

Crick, F. (1984). Function of the thalamic reticular complex: the searchlight hypothesis. *Proceedings of the National Academy of Sciences of the United States of America* **81**, 4586-90.

Dayan, P. and Abbott, L. F. (2001). Theoretical neuroscience : computational and mathematical modeling of neural systems. Cambridge, Mass.: Massachusetts Institute of Technology Press.

Diamond, M. E., von Heimendahl, M., Knutsen, P. M., Kleinfeld, D. and Ahissar, E. (2008). 'Where' and 'what' in the whisker sensorimotor system. *Nature Reviews Neuroscience* **9**, 601-12.

Doiron, B., Chacron, M. J., Maler, L., Longtin, A. and Bastian, J. (2003). Inhibitory feedback required for network oscillatory responses to communication but not prey stimuli. *Nature* **421**, 539-43.

Doiron, B., Laing, C., Longtin, A. and Maler, L. (2002). Ghostbursting: A novel neuronal burst mechanism. *Journal of Computational Neuroscience* **12**, 5-25.

Ermentrout, B., Pascal, M. and Gutkin, B. (2001). The effects of spike frequency adaptation and negative feedback on the synchronization of neural oscillators. *Neural Computation* **13**, 1285-310.

Fawcett, T. (2006). An introduction to ROC analysis. *Pattern Recognition Letters* **27**, 861-874.

Gabbiani, F., Metzner, W., Wessel, R. and Koch, C. (1996). From stimulus encoding to feature extraction in weakly electric fish. *Nature* **384**, 564-7.

Green, D. M. and Swets, J. A. (1966). Signal detection theory and psychophysics. New York. John Wiley and Sons.

Gussin, D., Benda, J. and Maler, L. (2007). Limits of linear rate coding of dynamic stimuli by electroreceptor afferents. *Journal of Neurophysiology* **97**, 2917-29.

Hagiwara, S., Szabo, T. and Enger, P. S. (1965). Electroreptors mechanisms in a high-frequency weakly electric fish *Sternarchus albifrons*. *Journal of Neurophysiology* **28**, 784-799.

Hand, D. J. and Till, R. J. (2001). A Simple Generalisation of the Area Under the ROC Curve for Multiple Class Classification Problems. *Machine Learning* **45**, 171-186.

Hanley, J. A. and McNeil, B. J. (1982). The meaning and use of the area under a receiver operating characteristic (ROC) curve. *Radiology* **143**, 29-36.

Heiligenberg, W. (1991). Neural nets in electric fish. Cambridge, Massachusetts. MIT Press.

Heiligenberg, W. and Dye, J. (1982). Labelling of electroreceptive afferents in a gymnotoid fish by intracellular injection of HRP: The mystery of multiple maps. *Journal of Comparative Physiology A: Neuroethology, Sensory, Neural, and Behavioral Physiology* **148**, 287-296.

Horowitz, P. and Hill, W. (1989). The art of electronics. Cambridge, UK. Cambridge University Press.

Hubel, D. H. and Wiesel, T. N. (1977). Ferrier lecture. Functional architecture of macaque monkey visual cortex. *Proceedings of the Royal Society of London. Series B: Biological Sciences* **198**, 1-59.

Jin, C. L., Ling, C. X., Huang, J. and Zhang, H. AUC: a Statistically Consistent and more Discriminating Measure than Accuracy. In *In Proceedings of 18th International Conference on Artificial Intelligence (IJCAI-2003)*, pp. 329-341.

Khanbabaie, R., Nesse, W. H., Longtin, A. and Maler, L. (2010). Kinetics of Fast Short-Term Depression Are Matched to Spike Train Statistics to Reduce Noise. *Journal of Neurophysiology* **103**, 3337-3348.

Kleinfeld, D., Ahissar, E. and Diamond, M. E. (2006). Active sensation: insights from the rodent vibrissa sensorimotor system. *Current Opinion in Neurobiology* **16**, 435-444.

Knudsen, E. I. (1975). Spatial aspects of electric fields generated by weakly electric fish. *Journal of Comparative Physiology* **99**, 103-118.

Knutsen, P. M. and Ahissar, E. (2009). Orthogonal coding of object location. *Trends in Neurosciences* **32**, 101-109.

Knutsen, P. M., Biess, A. and Ahissar, E. (2008). Vibrissal kinematics in 3D: tight coupling of azimuth, elevation, and torsion across different whisking modes. *Neuron* **59**, 35-42.

Kuhn, A., Aertsen, A. and Rotter, S. (2004). Neuronal integration of synaptic input in the fluctuation-driven regime. *Journal of Neuroscience* **24**, 2345-56.

Laing, C. R. and Longtin, A. (2003). Dynamics of Deterministic and Stochastic Paired Excitatory-Inhibitory Delayed Feedback. *Neural Computation* **15**, 2779-2822.

Lapicque, L. (1907). Recherches quantitatives sur l'excitation électrique des nerfs traitée comme une polarisation. *Journal du Physiologie et Pathologie Générale* **9**, 567-78.

Laurent, G. (2002). Olfactory network dynamics and the coding of multidimensional signals. *Nature Reviews Neuroscience* **3**, 884-95.

Lewis, J. E., Lindner, B., Laliberte, B. and Groothuis, S. (2007). Control of neuronal firing by dynamic parallel fiber feedback: implications for electrosensory reafference suppression. *Journal of Experimental Biology* **210**, 4437-4447.

Lewis, J. E. and Maler, L. (2001). Neuronal population codes and the perception of object distance in weakly electric fish. *Journal of Neuroscience* **21**, 2842-50.

Lewis, J. E. and Maler, L. (2002). Dynamics of electrosensory feedback: short-term plasticity and inhibition in a parallel fiber pathway. *Journal of Neurophysiology* **88**, 1695-706.

Lindner, B., Doiron, B. and Longtin, A. (2005). Theory of oscillatory firing induced by spatially correlated noise and delayed inhibitory feedback. *Physical Review E* **72**.

Ling, C., Huang, J. and Zhang, H. (2003). AUC: A Better Measure than Accuracy in Comparing Learning Algorithms. In *Advances in Artificial Intelligence*, vol. 2671 eds. Y. Xiang and B. Chaib-draa, pp. 991-991. Springer Berlin / Heidelberg.

Ludtke, N. and Nelson, M. E. (2006). Short-term synaptic plasticity can enhance weak signal detectability in nonrenewal spike trains. *Neural Computation* **18**, 2879-916.

Ma, J. and Wu, J. (2007). Multistability in spiking neuron models of delayed recurrent inhibitory loops. *Neural Computation* **19**, 2124-48.

MacIver, M. A., Sharabash, N. M. and Nelson, M. E. (2001). Prey-capture behavior in gymnotid electric fish: Motion analysis and effects of water conductivity. *Journal of Experimental Biology* **204**, 543-557.

Maler, L. (1979). The posterior lateral line lobe of certain gymnotoid fish: quantitative light microscopy. *Journal of Comparative Neurology* **183**, 323-363.

Maler, L. (2009a). Receptive field organization across multiple electrosensory maps. I. Columnar organization and estimation of receptive field size. *Journal of Comparative Neurology* **516**, 376-93.

Maler, L. (2009b). Receptive field organization across multiple electrosensory maps. II. Computational analysis of the effects of receptive field size on prey localization. *Journal of Comparative Neurology* **516**, 394-422.

Mann, H. B. and Whitney, D. R. (1947). On a Test of Whether one of Two Random Variables is Stochastically Larger than the Other. *The Annals of Mathematical Statistics* **18**, 50-60.

Metzner, W., Koch, C., Wessel, R. and Gabbiani, F. (1998). Feature extraction by burst-like spike patterns in multiple sensory maps. *Journal of Neuroscience* **18**, 2283-300.

Mileva, G., Zysman, D., Groothuis, S. and Lewis, J. E. (2008). In vitro studies of closed-loop feedback and electrosensory processing in Apteronotus leptorhynchus. *Journal of Physiology-Paris* **102**, 173-180.

Moller, P. (1995). Electric fishes : history and behavior. London, UK. Chapman & Hall.

Montgomery, J. C. and Bodznick, D. (1994). An adaptive filter that cancels self-induced noise in the electrosensory and lateral line mechanosensory systems of fish. *Neuroscience Letters* **174**, 145-148.

Montgomery, J. C. and Bodznick, D. (1999). Signals and noise in the elasmobranch electrosensory system. *Journal of Experimental Biology* **202**, 1349-1355.

Nelson, M. E. and Maciver, M. A. (1999). Prey capture in the weakly electric fish Apteronotus albifrons: sensory acquisition strategies and electrosensory consequences. *Journal of Experimental Biology* **202**, 1195-1203.

Nelson, M. E., MacIver, M. A. and Coombs, S. (2002). Modeling electrosensory and mechanosensory images during the predatory behavior of weakly electric fish. *Brain, Behavior and Evolution* **59**, 199-210.

Nelson, M. E., Xu, Z. and Payne, J. R. (1997). Characterization and modeling of P-type electrosensory afferent responses to amplitude modulations in a wave-type electric fish. *Journal of Comparative Physiology. A, Sensory, Neural, and Behavioral Physiology* **181**, 532-44.

Oswald, A. M., Chacron, M. J., Doiron, B., Bastian, J. and Maler, L. (2004). Parallel processing of sensory input by bursts and isolated spikes. *Journal of Neuroscience* **24**, 4351-62.

Oswald, A. M., Lewis, J. E. and Maler, L. (2002). Dynamically interacting processes underlie synaptic plasticity in a feedback pathway. *Journal of Neurophysiology* **87**, 2450-63.

Petersen, R. S., Panzeri, S. and Diamond, M. E. (2002). Population coding in somatosensory cortex. *Current Opinion in Neurobiology* **12**, 441-447.

Press, W. H., Teukolsky, S. A., Vetterling, W. T. and Flannery, B. P. (1992). Numerical recipes in C : the art of scientific computing. Cambridge, UK. Cambridge University Press.

Prinz, A. A., Abbott, L. F. and Marder, E. (2004). The dynamic clamp comes of age. *Trends in Neurosciences* **27**, 218-24.

Rechten, C., Avery, M. and Stevens, A. (1983). Optimal prey selection: Why do great tits show partial preferences? *Animal Behaviour* **31**, 576-584.

Rose, G. J. (2004). Insights into neural mechanisms and evolution of behaviour from electric fish. *Nature Reviews Neuroscience* **5**, 943-51.

Rosenblueth, A., Wiener, N. and Bigelow, J. (1943). Behavior, Purpose and Teleology. *Philosophy of Science* **10**, 18-24.

Sas, E. and Maler, L. (1983). The nucleus praeeminentialis: A Golgi study of a feedback center in the electrosensory system of gymnotid fish. *Journal of Comparative Neurology* **221**, 127-144.

Sas, E. and Maler, L. (1987). The organization of afferent input to the caudal lobe of the cerebellum of the gymnotid fish Apteronotus leptorhynchus. *Anatomy and Embryology* **177**, 55-79.

Saunders, J. and Bastian, J. (1984). The physiology and morphology of two types of electrosensory neurons in the weakly electric fish Apteronotus leptorhynchus. *Journal of Comparative Physiology. A, Sensory, Neural, and Behavioral Physiology* **154**, 199-209.

Sawtell, N. B., Williams, A. and Bell, C. C. (2005). From sparks to spikes: information processing in the electrosensory systems of fish. *Current Opinion in Neurobiology* **15**, 437-43.

Scheich, H., Bullock, T. H. and Hamstra Jr, R. H. (1973). Coding properties of two classes of afferent nerve fibers: high-frequency electroreceptors in the electric fish, Eigenmannia. *Journal of Neurophysiology* **36**, 39-60.

Sharp, A. A., O'Neil, M. B., Abbott, L. F. and Marder, E. (1993a). The dynamic clamp: artificial conductances in biological neurons. *Trends in Neurosciences* **16**, 389-94.

Sharp, A. A., O'Neil, M. B., Abbott, L. F. and Marder, E. (1993b). Dynamic clamp: computer-generated conductances in real neurons. *Journal of Neurophysiology* **69**, 992-5.

Sheskin, D. (2000). Handbook of parametric and nonparametric statistical procedures. Boca Raton, Florida. Chapman & Hall.

Smith, G. D. and Sherman, S. M. (2002). Detectability of Excitatory versus Inhibitory Drive in an Integrate-and-Fire-or-Burst Thalamocortical Relay Neuron Model. *Journal of Neuroscience* **22**, 10242-10250.

Stephens, D. W., Brown, J. S., Ydenberg, R. C. and Krebs, J. R. (2007). Foraging : behavior and ecology. Chicago, Illinois. University of Chicago Press.

Stephens, D. W. and Krebs, J. R. (1986). Foraging theory. Princeton, New Jersey. Princeton University Press.

Sutherland, C., Doiron, B. and Longtin, A. (2009). Feedback-induced gain control in stochastic spiking networks. *Biological Cybernetics* **100**, 475-89.

Theunissen, F. and Miller, J. P. (1995). Temporal encoding in nervous systems: A rigorous definition. *Journal of Computational Neuroscience* **2**, 149-162.

Wessel, R., Koch, C. and Gabbiani, F. (1996). Coding of time-varying electric field amplitude modulations in a wave-type electric fish. *Journal of Neurophysiology* **75**, 2280-2293.

Wiener, N. (1961). Cybernetics or control and communication in the animal and the machine. New York, New York. MITPress.

Wilcoxon, F. (1945). Individual Comparisons by Ranking Methods. *Biometrics Bulletin* **1**, 80-83.

Xu, Z., Payne, J. R. and Nelson, M. E. (1996). Logarithmic time course of sensory adaptation in electrosensory afferent nerve fibers in a weakly electric fish. *Journal of Neurophysiology* **76**, 2020-32.

Zupanc, G. and Bullock, T. (2005). From Electrogenesis to Electroreception: An Overview. In *Electroreception*, eds. T. H. Bullock C. D. Hopkins A. N. Popper and R. A. Fay, pp. 5-46. New York, New York. Springer.